

# **The Use of Spectral Unmixing of Landsat Imagery in Estimating Surface Runoff**

Nguyen Ngoc Anh

Thesis submitted in partial fulfilment of the requirements for the award of  
Masters of Geospatial Information Science

School of the Environment  
Faculty of Science and Engineering  
**Flinders University of South Australia**

# CONTENTS

<b>Declaration of Original Work .....</b>	<b>5</b>
<b>Acknowledgements .....</b>	<b>6</b>
<b>List of Figures .....</b>	<b>7</b>
<b>List of Tables.....</b>	<b>9</b>
<b>List of Abbreviations .....</b>	<b>10</b>
<b>Abstract .....</b>	<b>11</b>
<b>Keywords.....</b>	<b>13</b>
<b>Chapter 1 – Introduction .....</b>	<b>14</b>
1.1 Background of study.....	14
1.1 Problem statement .....	17
1.2 Research question .....	20
1.3 Research aims and objectives .....	20
1.4 Scope of study and anticipated outcomes.....	21
1.5 Thesis structure.....	22
<b>Chapter 2 – Literature Review.....</b>	<b>24</b>
2.1 Background of floods .....	24
2.2 Urban floods in developing and developed countries .....	25
2.2.1 Urban floods in developing countries.....	25
2.2.2 Urban floods in developed countries .....	26
2.3 The characteristics of urban environment .....	28
2.3.1 Urban characteristics .....	28
2.3.2 Adelaide metro area.....	29
2.4 Impervious surfaces and surface runoff .....	30
2.5 Remote sensing techniques in mapping land-cover .....	31
2.5.1 Mixed pixel.....	32
2.5.2 Hard classification.....	32

2.5.3 Soft classification .....	33
2.6 GIS applications in hydrological modelling.....	35
2.6.1 GIS data .....	35
2.6.2 Hydrological modelling with GIS .....	36
2.7 Hydrological model .....	37
2.7.1 Hydrological cycle and water balance.....	37
2.7.2 Application of WetSpa Model.....	39
<b>Chapter 3 - Study area and data .....</b>	<b>41</b>
3.1 The study area.....	41
3.1.1 Hydrogeological zones .....	42
3.1.2 Stormwater in Adelaide .....	43
3.2 Data.....	44
3.2.1 Landsat surface reflectance imagery .....	44
3.2.2 Land-cover map.....	46
3.2.3 Land use.....	46
3.2.4 Elevation data .....	46
3.2.5 Slope .....	47
3.2.6 Soil.....	48
3.2.7 Rainfall map .....	49
3.2.8 Temperature.....	50
3.2.9 Wind .....	50
3.2.10 Potential Evapotranspiration (Pet).....	50
3.2.11 Groundwater Depth .....	51
<b>Chapter 4 - Methodology .....</b>	<b>52</b>
4.1 Remote sensing method.....	52
4.1.1 Subset image.....	52
4.1.2 Supervised classification .....	52

4.1.3 Spectral Unmixing.....	54
4.2 GIS method.....	56
4.2.1 Kriging.....	56
4.2.2 Inverse Distance Weighting (IDW).....	57
4.2.3 Recoding the data .....	58
4.3 The WetSpass model .....	59
4.3.1 Model concept .....	59
4.3.2 Calculating water balance for each raster cell.....	60
4.3.3 Calculating Surface runoff .....	60
<b>Chapter 5 - Results .....</b>	<b>63</b>
5.1 Land use map.....	63
5.2 Spectral Unmixing Analysis results .....	64
5.2.1 Endmember selection .....	64
5.2.2 Endmember abundance maps .....	66
5.3 Spatial distribution of surface runoff.....	69
5.3.1 Monthly surface runoff patterns .....	69
5.3.2 Annual surface runoff distribution .....	72
<b>Chapter 6 - Discussion.....</b>	<b>77</b>
6.1 General findings .....	77
6.1.1 Spectral Unmixing Analysis.....	77
6.1.2 Spatial distribution Surface runoff volume .....	78
6.1.3 Comparisons between two approaches.....	82
6.1.4 Areas vulnerable to surface runoff and flooding.....	89
6.2 Limitations.....	91
<b>Chapter 7 - Conclusion.....</b>	<b>94</b>
<b>References.....</b>	<b>98</b>
<b>Appendices .....</b>	<b>105</b>

## **Declaration of Original Work**

I hereby declare that the following thesis is a product of my own research. All information contained within this document is original work and to the best of my knowledge has not featured in any other published and unpublished literature, except where due reference has been given in the text.

Nguyen Ngoc Anh

.....

November, 2016

## **Acknowledgements**

First of all, I would like to give thanks to Australia Award Scholarship for giving me the opportunity to pursue my dream of studying in Australia and to gain valuable knowledge from the Master of Geospatial Information Science course.

I would like to give many thanks to my supervisor as well as the GIS program coordinator, Mr Stephen Fildes, for his support in my course time, especially for his guidance and discussion in this research. My special thanks to Mr Robert Keane who introduced me to spatial data management and his guidance for my thesis. Also much thanks to Dr Mark Lethbridge who helped me to gain the valuable knowledge in GIS modelling and spatial statistics. This helped me to be more confident when working with GIS data.

My special thanks to my wife, Nguyen Thi Thu Ha, my family and my special friend, Dang Phuong Loan, who always encouraged and supported me during the study time at Flinders University. I could never have finished my study without all of their contributions.

## List of Figures

<b>Figure 2.1.</b> Hydrological cycle (Zhang, Walker & Dawes 2002) .....	38
<b>Figure 3.1.</b> The study area .....	41
<b>Figure 3.2.</b> Hydrogeological zones (Gerges 2006).....	43
<b>Figure 3.3.</b> Landsat scene path 97, row 84 .....	45
<b>Figure 3.4.</b> The DEM of the study area .....	47
<b>Figure 3.5.</b> Slope data of the study area .....	48
<b>Figure 3.6.</b> Soil types in the study area.....	49
<b>Figure 3.7.</b> Groundwater depth across the study area .....	51
<b>Figure 4.1.</b> Neighbourhood (red points) for selected point (yellow point) .....	57
<b>Figure 5.1.</b> Land-use map of the study area .....	63
<b>Figure 5.2.</b> Spectral reflectance of vegetation (a), bare soil (b) and impervious surface (c) at six spectral bands of the image .....	65
<b>Figure 5.3.</b> Fractional maps of vegetation, bare soil, open water and impervious surfaces .....	68
<b>Figure 5.4.</b> Spatial patterns of surface runoff 2016 over metropolitan Adelaide using land-use types and default land cover fractions .....	70
<b>Figure 5.5.</b> Monthly spatial distribution of surface runoff 2016 using fractional maps derived from Spectral Unmixing .....	71
<b>Figure 5.6.</b> Annual surface runoff 2016 using land-use map: a) – The whole study area; b) – The highest annual runoff in the inland area (red colour).....	73
<b>Figure 5.7.</b> The lowest values of annual surface runoff .....	74
<b>Figure 5.8.</b> Annual surface runoff 2016 using fractional maps of Spectral Unmixing Analysis: a) – For the whole study area, b) – The highest annual runoff across the study area.....	75

<b>Figure 5.9.</b> The lowest values of annual surface runoff resulting from Spectral Unmixing Analysis .....	76
<b>Figure 6.1.</b> Proportions of vegetation, bare soil and impervious surfaces covering each ‘impervious’ land-use type .....	77
<b>Figure 6.2.</b> Surface runoff distribution and soil types in the study area in July, 2016 (surface runoff map + soil map + overlaid soil map and surface runoff map) .....	78
<b>Figure 6.3.</b> Mixed vegetation, soil and impervious surfaces in one land-use type .....	80
<b>Figure 6.4.</b> Homogeneous pixels in surface runoff map of July and the corresponding land cover .....	81
<b>Figure 6.5.</b> Heterogeneous pixels in surface runoff map of July and the corresponding land cover .....	82
<b>Figure 6.6.</b> Surface runoff in a heterogeneous area resulting from the two approaches .....	84
<b>Figure 6.7.</b> Mean values of monthly surface runoff resulting from using land-use map and fractional maps from Spectral Unmixing Analysis in 2016 .....	85
<b>Figure 6.8.</b> Differences between annual surface runoff of WetSpss using Spectral Unmixing Analysis and Land-use data.....	86
<b>Figure 6.9.</b> Open water and mixed water-vegetation-bare soil areas marked on Landsat 8 Reflectance Image .....	88
<b>Figure 6.10.</b> Areas vulnerable to flooding based on surface runoff volume .....	91

## List of Tables

<b>Table 3.1.</b> Spectral bands of Landsat 8 imagery used in the research .....	46
<b>Table 3.2.</b> Average monthly maximum and minimum temperature at 8 observed stations across the study area in 2016.....	50
<b>Table 3.3.</b> Average monthly potential evapotranspiration in Adelaide metropolitan area 2016 .....	51
<b>Table 4.1.</b> Derived land-use types of the study area and corresponding information in the WetSpaas model.....	58
<b>Table 5.1.</b> Land use types in the study area.....	64
<b>Table 5.2.</b> Statistics of selected vegetation endmember .....	66
<b>Table 5.3.</b> Statistics of selected bare soil endmember .....	66
<b>Table 5.4.</b> Statistics of selected impervious surface endmember .....	66
<b>Table 5.5.</b> Mean values of vegetation, bare soil, open water and impervious surfaces over the study area.....	69

## List of Abbreviations

RS	Remote Sensing
GIS	Geographical Information System
WetSpass	Water and Energy Transfer between Soil, Plants, and Atmosphere under quasi-Steady State
LULC	Land-use/Land-cover
LU	Land use
LC	Land cover
LMM	Linear mixture model
SUA	Spectral Unmixing Analysis
RMSE	Root Mean Square of error
NDBI	Normalized Difference Built-up Index
NDVI	Normalized Difference Vegetation Index

## **Abstract**

Urbanization and urban expansion has been a widely recognized problem throughout the world due to its negative influences on of land-use/land-cover changes. The growth of urbanization leads to impervious surfaces replacing natural landscapes. As impervious surfaces increase, surface runoff produced from rainfall and other sources also increases. This is one of the primary cause of urban flooding.

Adelaide metropolitan area is the capital city of South Australia. The city is in a low-lying region and upstream catchments flow across the urban area. It still has much of the original stormwater drainage infrastructure, which was built in the period of 1940s to 1980s and the drainage systems have not been frequently reconstructed. This leads to an inadequate flow capacity or lack of drainage infrastructure, resulting in the increase of surface runoff and vulnerability to flooding.

WetSpass model developed by Batelaan and De Smedt in 2001 is used for estimating surface runoff based on a water balance calculation. It assumes that each pixel in a land-use map contains proportions of land cover types (endmember), that are more or less conducive to surface water runoff; these include vegetation, impervious surfaces, bare soil, and open water. The proportions of those contributions are assumed to be the same for every pixel in a land-cover category. This could be subjective when applying the model to different study areas due to different characteristics of the landscape.

This research introduces the use of Spectral Unmixing of Landsat imagery to produce fractional maps of these endmembers as substitute for using the land-use category alone in order to improve the efficiency of WetSpass model in estimating surface runoff over

the Adelaide metropolitan area. The result of surface runoff estimation is used to help in indicating the areas vulnerable to flooding in the study area.

## **Keywords**

RS, GIS, WetSpass, Flood, Spectral Unmixing, SUA, LULC, Adelaide

# **Chapter 1 – Introduction**

## **1.1 Background of study**

Urbanization has been a widely recognized problem around the world due to its negative influences on land use/land-cover (LULC) changes. As urbanization increases, natural environs and agricultural lands will be steadily replaced by impervious surfaces resulting in increases in the amount, intensity and duration of surface runoff (Weng 2001). According to Bauer et al. (2008), the expansion of impermeable surfaces is the primary factor affecting the water quality of streams and lakes as well as volumes of stormwater runoff in urban areas raising flooding risks.

Surface runoff or overland flow is known as the water derived from different sources like rainfall or snowmelts that flow over landscapes. This phenomenon occurs when the amount of water infiltrated by the surface and evaporated to the atmosphere is smaller than that of the water falling on the ground (Pidwirny 2006). In urban areas, the urban landscapes often contain a high density of manmade objects such as buildings, concretes and roads where water is unable to infiltrate into the soil causing surface runoff and it is considered the major cause of urban flooding (Chen et al. 2009).

Over the last twenty years, there has been a significant increase in flooding events reported. Jha et al. (2012) in the report named “Cities and Flooding, A Guide to Integrated Urban Flood Risk Management for the 21st Century” show that people affected by flooding in 1990 are around 50 million. It rapidly increased to 178 million in 2010. In Australia, despite the benefit of preparedness to adapt to environmental impacts, flooding still causes substantial damages for economic, social and

environmental aspects every year. It directly damages residential, commercial, industrial and recreational buildings, critical infrastructure, equipment and facilities, and causes injury and death and polluted water supplies (Commonwealth of Australia 2009).

Adelaide is the capital city of South Australia with a population around 1.32 million people, while the population of South Australia is approximately 1.7 million in 2015 (ABS 2016). According to Wright and Kemp (2016), this city is in a low-lying region and flash floods are a problem most commonly experienced in the urban environment. As many rural areas are located in the higher-lying regions, in many cases, upstream catchments flow down into urban areas. They also indicate that some urbanized areas are likely to be affected by overland flow that does not originate from the creek system. This might lead to the increase of flood risks in metropolitan Adelaide. In addition, Adelaide metropolitan area contains much of original stormwater drainage infrastructure, which were built in the period of 1940s to 1980s. Those systems were designed and relied on an assumed percentage of impermeable surfaces, which was derived from early predictions of urban development at the time of design. Some significant improvement based on rainfall intensity and a catchment response have been created over time. However, the drainage systems have not catered for increases in urban infill and development since the 1980s (Parliament of Australia 2015). This could lead to an inadequate flow capacity or a lack of drainage infrastructure in the context of a higher population living in the metropolitan Adelaide and thus resulting in increasing surface runoff and vulnerability of flooding.

There are different hydrological models that can be used for estimating the surface runoff distribution varying over space. One such model is WetSpass (Water and Energy Transfer between Soil, Plants, and Atmosphere under quasi-Steady State) developed by Batelaan and De Smedt (2001), which is integrated into a geographical information system (GIS) as a raster-based model. WetSpass is used for estimating spatial distributions of groundwater recharge, surface runoff, and evapotranspiration by investigating physical and empirical relationships over a long-term. When this model was published, several studies have relied on it for understanding the hydrological process in urban areas. Poelmans et al. (2010) couple WetSpass model and urban expansion models in order to evaluate the significance of scale effects, while Al Kuisi and El-Naqa (2013) utilize this model to estimate spatial groundwater recharge in the Jafr basin, Jordan. WetSpass considers LULC as an important factor in its operation. It assumes that an individual LULC unit contains fractions of Vegetation, Soil, Impervious Surface, and Open Water. The sum of those fractions is equal to 1 or 100 percent. By using vegetated, impervious area, soil and open-water fractions present within each pixel in WetSpass, the mixed-pixel problem can be solved (Batelaan & De Smedt 2001).

Surface runoff estimation for preventing flood hazards in the future by accessing the influence of LULC changes is challenging in many research (Breuer et al. 2009). Recently, remote sensing (RS) is known as the most common data source, which is used to detect, quantify and map LULC patterns and changes due to the repetition of data acquisition, data format and the accuracy of georeferencing procedures (Jensen 2005; Lu et al. 2004). Many satellite programs are currently in operation. However, for the

studies in change detection, the Landsat system is a the unique program which supports a historical and continuous record of imagery (El-Kawy et al. 2011). Consequently, Landsat imagery is a viable approach to obtaining data that is repetable and suitable for hydrological models. By using Landsat images, LULC can be mapped repeatably over large areas, helping in mapping, monitoring and managing LULC changes (Wulder et al. 2008). This largely includes changes of impervious areas typical of many LULC types that cause surface runoff. These changes changes can be derived from Landsat data with appropriate image analysis methods. Monitoring the spatial distribution of surface runoff will help to indicate the areas vulnerable to flooding in urban areas in general and in the metropolitan Adelaide in particular.

### **1.1 Problem statement**

Urbanization causes an increase of flood risk in cities because of local changes in hydrological conditions. Accompanying urbanization is an increase in the population living in cities. According to the Uunited Nations (2006), an increase in population in urban areaqs more likely occurs in developing countries rather than in developed countries and at a more rapid rate. Consequently, with increasing human settlements, infrastructure development and industrial growth, the sprawl of urban areas is often uncontrolled. Urban development also causes LULC changes, resulting in changes of hydrological conditions and increase of flood hazard. This is particularly true in the author's home country of Vietnam and cities like Ho Chi Minh City where a lack of urban stormwater infrastructure results in sevier flooding during and after large rainfall events.

In tropical and developing countries such as Vietnam, the annual rainfall is significant. According to Vietnam Government Portal (2016), the annual rainfall in Vietnam is from 1500 to 2000 mm with the humidity is around 80%. Vietnam is also one of the countries affected by El Niño events which cause the increase of rainfall intensity. Furthermore, Vietnam is also struck by four to six typhoons every year on average (Garcia 2002). Most large cities like Hanoi and Ho Chi Minh City in Vietnam are in low-lying regions with poor quality of infrastructure. In the context of climate change, the country likely suffers from different types of natural disasters and one of the most common and serious being flooding (Navrud et al. 2012). These problems increasingly cause flood risks in both frequency and severity. In addition, there are few studies focused on floods in Vietnam urban environments where the development of stormwater and flood mitigation infrastructure has not kept pace with urban development. Therefore, it is necessary to investigate vulnerability to urban flooding in Vietnam through applying techniques for estimating surface runoff changes over time. However, the data in Vietnam used in this research are limited due to its scarcity and lower accuracy. While the author of this research is employed by the Vietnam's Ministry of Natural and Resources and Environment, it is difficult to obtain the required spatial datasets from relevant government authorities without being present in the country. Moreover, to collect enough data in Vietnam to support this research, it also required field-data collection and contacts with Vietnamese authorities. This proved too costly and consumed a large amount of time. Thus, this research focussed on applying methods for surface runoff estimation in metropolitan Adelaide, South Australia where the urban area is dominant and flood often occurs in the rainy season. The intent is to develop

methods that are transferable to other urban cities like those of the author's home country.

Like other hydrological models that are applied to calculate water balance components in different areas, the WetSpass model provides spatial distributed surface runoff raster maps by using highly relevant input data such as elevation, soil, LULC and climate data (rainfall, temperature and wind speed) (Batelaan & De Smedt 2001). However, the model uses the default material fractions of LULC types (vegetated, soil, impervious and open water area) within a regular spatial unit (pixel) in its operation. This could be subjective when applied to different study areas due to the different contributions of these materials. Therefore, the estimation of material proportions at the pixel level for a particular study area will help to improve the efficiency of WetSpass model.

Furthermore, as mentioned earlier, LULC plays a significant role in generating surface runoff and it is an indispensable component in the input data of WetSpass. In mapping LULC patterns, remotely sensed data is considered as the most common data source (Lu et al. 2004) and depending upon a sufficient understanding of landscape characteristics, imaging systems, and information extraction techniques that be used to employ in the relation to the analyzing aim (Yang, X & Lo 2002). Nowadays, remote sensing data with high spatial and spectral resolution can be used for mapping LULC. However, compared to medium resolution imagery, this kind of data has some disadvantages, for example, its high cost, low temporal resolution, and relatively small footprint. In addition, hard and soft classification are the two most common methods to derived LULC from remotely sensed data. However, hard classification approach has a significant disadvantage when working with heterogeneous land scapes such as urban

environments where a single pixel contains a mix of land cover types, while soft classification method is able to solve this problem (Binaghi et al. 1999; Foody & Cox 1994). The basic idea of soft classification method is that proportions of more than one land-cover type within a pixel can be extracted by using spectral compositions. Spectral Unmixing is a technique that can calculate the proportion of each contribution like Vegetation, Soil, Impervious Surface, and Open Water in each pixel and produce fractional maps of these categories that may improve the WetSpass model. As Canters et al. (2011) and Montzka et al. (2008) show, improving the parameterization of urban LULC results will significantly improve the predictions of the hydrological model.

## **1.2 Research question**

Specifically, this research attempts to answer these following questions:

- Can Spectral Unmixing of Landsat imagery help identify the key spectral parameter of Soil Vegetation, Open Water and Impervious Surface for runoff estimation?
- Is the result of Spectral Unmixing Analysis applied with multispectral imagery reliable?
- Which approach, WetSpass using Spectral Unmixing Analysis or using the default land-use setting, is better?
- Where are the areas vulnerable to surface runoff and flooding?

## **1.3 Research aims and objectives**

From the research questions posed, the primary aim of this study is to model the monthly and annual spatial distribution in runoff potential to help in identifying areas vulnerable to surface runoff and flooding in metropolitan Adelaide.

The objectives of the research are:

- To create the necessary input data for the WetSpa model from raw data.
- To spectrally unmix Landsat imagery to identify the key spectral parameters of Vegetation, Soil, Water and Impervious surfaces for runoff estimation.
- To map changes in the spatial distribution of surface runoff of metropolitan Adelaide over a 12-month period in 2016.
- Compare surface runoff results between default fractions of vegetation, bare soil, surface runoff and open water with the abundance results of those components from the Spectral Unmixing Analysis.

#### **1.4 Scope of study and anticipated outcomes**

This research examines the use of spectral unmixing of Landsat imagery in estimating surface runoff in metropolitan Adelaide, South Australia with the intent of apply the methodology and findings to Ho Chi Minh City where urban floods occur frequently and causing serious damage to property and life during the rainy season (from May to November). This city is characterized by unplanned developments with poor stormwater drainage. The contribution of impervious surface runoff that exacerbates flooding in this urban area is significant. However, due to the limited time for conducting this research, in the data collection stage, the author could not collect enough input data for running the hydrological model on Ho Chi Minh City. Therefore, the study area was moved to metropolitan Adelaide where key data sets are available and reliable. After implementing this research in the Adelaide region, it is expected the methods used in this study will be applied in some urban areas in Vietnam, especially in Ho Chi Minh City.

Irrespective of the location, this study investigates the use of Spectral Unmixing Analysis in estimating the spatial distribution of surface runoff and those areas potentially vulnerable to surface runoff and flooding. The results of this study will be used to identify the areas vulnerable to surface runoff and flooding in metropolitan Adelaide. Consequently, some prioritising flood mitigation measures should be considered based on the current status of those areas. This is also illustrates the application of remote sensing method coupling with a hydrological model in order to achieve a better result. Spectral Unmixing method can also help in exploring urban composition using remotely sensed information at a single pixel scale. It is possibly meaningful for urban planners in monitoring urban expansion based on the changes of impervious element resulting from this method.

### **1.5 Thesis structure**

Chapter 2 of this thesis will provide general information about floods; discuss characteristics of floods in developing and developed countries; illustrate the characteristics of the urban environment and metropolitan Adelaide; point out the relationship between impervious surfaces and surface runoff. Chapter 2 also shows a review of remote sensing techniques in investigating LULC including revealing the mixed pixel problem, hard and soft classification in mapping LULC. Finally, the background of the hydrological cycle and water balance and the application of WetSpas model in different studies will be demonstrated.

Chapter 3 describes the study area where the research will be applied and a description of the input data for the WetSpas model to estimate surface runoff across metropolitan Adelaide.

Chapter 4 focuses on describing the methods that have been used when conducting this research. It illustrates the principle of remote sensing methods like such as supervised classification and spectral unmixing analysis; GIS methods and the WetSpass model calculations.

Chapter 5 presents the results of this study including a land-use map derived from coupling an original land-use map and a land-cover map, which is the result of a supervised classification approach; the abundance maps of four endmembers, including vegetation, bare soil, impervious surfaces and open water and the distribution of surface runoff monthly and annually over the study area. Surface runoff maps include the results of two methods, which use land-use map and the fractional maps as input data to the WetSpass model.

Chapter 6 provides a discussion based on the results with general findings, limitations and considerations for the future studies.

Chapter 7 concludes the thesis and proposes some recommendations.

## **Chapter 2 – Literature Review**

### **2.1 Background of floods**

Flooding comprises 32 percent of all natural disasters and is the most well-known (Eisensee & Strömberg 2007). As Jonkman (2005) indicates, floods are responsible for enormous damage throughout the world every year. Floods killed approximately 100,000 and affected over 1.4 billion people over the last decade of the twentieth century.

There are various definitions used to describe floods based on the purposes of research and the context used (Brooks 2003; World Health Organization 2013). According to National Geographic (nd), flooding occurs when water overflows or inundates land that is normally dry and this phenomenon can occur in different ways. There are different flooding kinds such as river floods, coastal floods, flash floods and urban floods.

The U.S. Department of Commerce (2005) illustrates that river floods are the inundation over a normally dry area due to the increasing level of water level in an established watercourse. River floods form with slow speed and cause less fatalities, however, their effects can spread across large areas with much damage (Klijn 2009).

Flash floods relate to the rapid rise of water in low-lying urbanized areas or along streams and creeks. This kind of flood often develops in less than six hours (Bureau of Meteorology 2016) and it is the most common form experienced in urban areas of South Australia (Wright & Kemp 2016).

Coastal floods are often the result of extreme storm events accompanying by strong onshore coastal winds and vast waves and high tides. This causes floods at coastal zones and estuaries with ocean water (Klijn 2009).

Lastly, urban floods can be caused by river floods, flash floods or coastal floods due to the poor condition of drainage systems, and impervious surfaces accompanied by high intensity of rainfall. In most cases where urban floods occur, those urban areas are often characterized by sealed surfaces that reduce the infiltration along with poor drainage system (Chen, Hill & Urbano 2009).

## **2.2 Urban floods in developing and developed countries**

### **2.2.1 Urban floods in developing countries**

Urban development in developing countries are characterized by the high density of population concentrated in a small area with poor public transportation, lack of sewage and stormwater facilities and air and water pollution (Szöllösi-Nagy & Zevenbergen 2005). Main causes of flooding in developing countries is that of uncontrolled urban development that occurs rapidly and unpredictably. Urban development tendency in developing countries often commence downstream then move upstream leading to rising damage impacts (Dunne 1986). WHO (1988) also indicates that the population in peri-urban and risk regions (flood plains and hillside areas) often has low income and is living in poorly constructed dwellings and occupy other infrastructure in poor condition. Furthermore, the cities and population usually cannot afford to supply the fundamental needs of water, drainage as well as sanitation due to lack of sufficient funds (Szöllösi-Nagy & Zevenbergen 2005). Those problems prevent the possibility of adequate water drainage during storms or heavy rain periods of any duration. In

addition, when undertaking flood research in some developing countries like India, Bangladesh, and Nepal, Mirza (2011) poses that precipitation significantly causes flooding in those countries because over 80 percent of the rainfall falls intensity in the rainy months (from June to September). Most floods occur in every river basin where the intensive rainfall is high during July and August.

Vietnam is characterized by the tropical monsoon climate where the annual rainfall is between 1500 and 2000 mm and the humidity is around 80% (Vietnam Government Portal 2016). The country is likely to suffer from different types of natural disasters with flooding is the most common and serious (Navrud et al. 2012). Largest cities in Vietnam such as Hanoi, Hai Phong, Ho Chi Minh City and Can Tho are in low-lying areas with poor condition of stormwater drainage. According to Storch and Downes (2011), only 28 percent of the current urban area of Ho Chi Minh City lies 2 meters above the sea-level and around 58% is above 1 m causing the city to be extremely vulnerable to inundation under the context of climate change. In Hanoi, as Bich et al. (2011) argue, the long and heavy rainfall in November 2008 led to the most devastating flood since 1973 for the capital city. This caused 90 inundated locations within Hanoi with the depth from 0.3m to 2.5m, 22 persons died and 3 were injured. It also significantly impacted health, social, economic, environmental of citizens living in Hanoi for a long term (Hanoi capital city's People Committee 2008).

### **2.2.2 Urban floods in developed countries**

Differently to developing countries, the waste process system and drainage systems in most developed countries are in a relatively good condition (Szöllösi-Nagy & Zevenbergen 2005). Those nations often have much better preparation in managing the

consequences of natural disasters in which flooding is the majority. Notably, 95 percent of the deaths caused by flood disasters is in developing countries (Price & Vojinovic 2008). According to Douben (2006), flooding duration in developed nations is usually relatively short. This is possibly because the flood mitigation activities in developed countries is better. They also have good policies to adapt to climate change and flooding risks such as providing future scenarios for dealing with flooding, balancing between adaptation and mitigation (Hamin & Gurran 2009).

In Australia, as Attorney-General's Department (nd) indicates, flooding occurring along watercourses after heavy rain is the most common form recorded. Furthermore, in some urban areas with high density of population, drainage systems can overflow, also causing floods. For coastal areas that are low-lying, storms and tropical cyclones can cause inundation in those areas.

Floods in Australia are grouped into three categories, slow onset flooding, quick onset flooding and flash flooding. The first type often occurs in Queensland, the West of New South Wales, some regions of North West Victoria and Western Australia. The duration of this flooding type is often in one or more weeks. In some cases, the flooding duration can happen lasting months. The effects of this flooding type typically include losing crops and livestock, disconnecting the traffic systems and isolating some whole communities. Quick onset flooding often occurs quickly in the mountain watershed area of large rivers and the rivers that drain to coastal areas. The duration of this flooding type can sometimes last for only one or two days. Because this form of flooding occurs quickly, there is less time for preventative actions. Therefore, it potentially causes significant risks to losing life and property. This flooding type often affects cities and

major towns, more frequently occurs in South Australia and Tasmania. Flash flooding occurs in a relatively short time, resulting from heavy rainfall and thunderstorms. It can occur in urbanized areas if the drainage systems in those areas cannot cope. Furthermore, flash flooding is also able to occur in un-urbanized areas due to the characteristics of natural terrain and steepness of streams in those areas.

## **2.3 The characteristics of urban environment**

### **2.3.1 Urban characteristics**

Urban ecosystems are characterized by humanity's impact on the environment where usually there are heterogeneous landscapes like roads, buildings, concretes, trees, grass, water, soil, and so on. Urban landscapes can be categorized into two types, built urban environment and the natural urban environment. The former involves man-made infrastructures like residential areas, transportation systems and buildings and the latter concerns parks, native vegetation areas and river surfaces. Generally, urban development has significant impacts on the changes of land cover types at local, regional and global scales (Xian 2015). As urban growth changes, urban infrastructure will alter natural features resulting in significantly changing urban landscapes from natural to anthropogenic impervious surfaces.

Nowadays, the population of the world living in urban areas is about 54% (UN 2015) and in the next 40 years, it is estimated that the population living in expanding urban centers will increase to two-thirds of the total (UN 2009). As the growth of population in metropolitans and the increasing influence of climate change, flooding risks and the expansion of pollution when flooding occurs is gradually increasing. Furthermore, as indicated by Güneralp, Güneralp and Liu (2015), coastal urban areas will be expanding

through vulnerable regions of low elevation with higher frequency of flooding. Heavy rain over upstream areas and the complexities in urban land-cover and drainage systems inherently affect surface runoff and pose challenges in predicting flood risk (Chen, Hill & Urbano 2009).

### **2.3.2 Adelaide metro area**

Adelaide's annual rainfall is around 600mm and mainly falls in the months of the winter months (June, July and August) with storms of high intensity that cause flooding problems, which also infrequently happen in the summer months (Kellogg Brown & Root Pty Ltd 2004). As Wright and Kemp (2016) pose, metropolitan Adelaide is lying on a floodplain leading to high flood risk. In most cases, the flood risk is flash floods, which are developed in an hour or less due to the small basin areas (catchment areas are often about 10 to 20 km<sup>2</sup>) where the streams often flow from rural upper catchments through urbanized areas. In addition, many sections of creeks belong privately owned lands leading to difficulties in maximizing the flood capacity of channel maintenance. For example, removing debris and waste in the stream channel, and opening the channel space. Due to these problems with the rapid formation of flash floods, there is a need to calculate surface runoff estimation as a reference for monitoring and predicting flood risk.

Wilkinson et al. (2004) shows the relationship between urbanization and rainfall season in metropolitan Adelaide. According to these authors, land-use has heavy influences on water flow. In this zone, the catchments with heavy urbanization are affected by rainfall intensity whereas catchments predominated by rural areas experience extreme water deficit due to a lack of soil moisture where significant runoff is only produced by rural

catchments in the later months of the winter (from July to October). The writers also indicate the empirical result that impervious surfaces are an integral part of estimating annual rainfall flow. By using the volumetric runoff coefficient (VRC), a calculation of rainfall, which falls on each basin and actually flows to the drainage system then contributes to runoff to the sea can be made. They indicate that the VRC is greater when the proportion of impervious surfaces is high and it is lower in un-urbanised areas.

Other research focuses on flood hazard assessment at Port Adelaide and Brown Hill and Keswick Creek. According to Russell and Drew (2006), Port Adelaide Enfield coastal areas contain land portions that are low-lying. Some of these areas are significantly affected by vast tide levels. They found that stormwater heavily affects the low-lying land in Port Adelaide Enfield. The single flood flow path was not clear because the local catchments are extremely flat. Therefore, it needs a rigorous assessment of influences from larger storm events. The Government of South Australia (2013) indicates that some areas in metropolitan Adelaide have a mixture of urban and rural areas resulting in significant flooding during storms. Most of the lower catchment in Adelaide region is urbanized. As a consequence, flooding typically occurs when reaches of water ways are lower during the storms that have shorter duration.

#### **2.4 Impervious surfaces and surface runoff**

According to Arnold and Gibbons (1996), and Slonecker et al. 2001, impervious surfaces are the materials that prevent the water infiltration into the soil leading to changes in the flow dynamics and sedimentation of stormwater runoff. There are different materials presenting impervious surfaces. Some are easy to identify and the most prevalent are roads, rooftops, and others such as sidewalks, patios, bedrock

outcrops and compacted soil. Because impervious areas prevent infiltration and usually have a small initial storage, those surfaces consequently contribute runoff quicker and at a higher rate (Boyd, Bufill & Knee 1993), and reduce the time of runoff concentration leading to higher and sooner peak discharges after rainfall starts in basins (Weng 2001).

Surface runoff is the water flowing over the surface of the ground towards the stream channel (Rumynin, 2015). Freeze (1974) shows that surface runoff is generated from upland areas and its intensity depends on topography, soil characteristics, LULC and climate such as precipitation, temperature and wind. Those factors need to be considered in any hydrological model. In urban areas, trees and vegetation removal as well as street and house construction can lead to increases in impervious surfaces resulting in decreasing infiltration, lower groundwater table and increasing storm flows. In addition, impermeable surfaces are able to affect local streams like streamflow and water quality as well as flooding characteristics. Those conditions result in increasing the intensity of surface runoff during heavy rains and storms.

## **2.5 Remote sensing techniques in mapping land-cover**

Land-cover can be used to estimate the abundance of impervious surfaces across a landscape and is considered to be a fundamental variable. However, mapping and monitoring land-cover changes in urban environments with medium and coarse spatial resolution imagery is challenging because of the problems causing by mixed-pixels (Lu et al. 2011), especially in Landsat TM data (Lu & Weng 2004).

### **2.5.1 Mixed pixel**

Traditional image analysis techniques assume that an area represented in each pixel belongs to a unique land cover type. However, Fisher (1997) argues that the landscape, in reality, does not fit into the elemental squares of the finest pixel. As a result, land-cover information needs to be extracted by assumption that one pixel contains more than one land-cover type. Cracknell (1998), inheriting Fisher's research, demonstrates that if the land forms observed are plains, desert and water, the result could be improved because those are homogeneous surfaces over an area. Foody (2004) more illustrates that the sensor primarily defines the spatial unit or the pixel in other words. Consequently, the pixel is an arbitrary spatial unit. Furthermore, fundamental attributes of a pixel like shape, size and location are mainly determined by the sensor and not directly by the ground's properties. In general, there is more than one thematic class contained in one pixel of an image. If conventional approaches are used, mapping using remotely sensed data could lead to errors where mixed pixels are present. There are two approaches of imperviousness extraction, which are hard and soft classification.

### **2.5.2 Hard classification**

According to Lu and Weng (2007), in hard classification approach, the spectral information of all pixels in the training set are used for developing a signature of a given class. Therefore, all materials that are present inside the training pixel set contribute to the resulting signature and the impact of mixed pixels is omitted. Myint et al. (2013) further demonstrate that individual features of an urban landscape often have different size and shape to that of the image pixels. If the spatial resolution is refined and the area of the pixel is reduced, the accuracy of classification might not improve. In the case that

pixels are smaller than urban objects, this probably leads to additional spectral noise. Therefore, when working with urban environments, the hard classification method may be a disadvantage. Liu, Zhang and Wu (2011) indicate that hard classification is likely to work better over larger homogeneous areas and where adjacent classes are clearly separated.

### **2.5.3 Soft classification**

As mentioned above, the hard classification approach assumes the land-cover categories are mutually exclusive and classifies each pixel into one class. However, urban landscapes are mostly heterogeneous, and where the spatial resolution of remotely sensed images is limited by medium and coarse spatial resolution data, mixed pixels will occur (Lu & Weng 2007). Fisher (1997) and Cracknell (1998) point out a major problem that the presence of mixed pixels limit the effective use of remotely sensed data in hard classification, especially in urban environments where they primarily contain impervious surface materials with the heterogeneity and complexity. Despite the fact that there are different methods used to derive the allocation of those pixels, they are still inappropriately allocated in a single class.

Ridd (1995) proposed that vegetation, soil and impervious surfaces are three land-cover elements that contribute to the spatial component of a segment of an urban environment, which is called VIS (Vegetation, Impervious Surfaces and Soil) model. According to this model, each subdivision of an urban area can be calculated based on the contribution of vegetation, soil, and impervious surface within each spatial unit. When the changes of VIS constituency are observed over the time, the VIS model not only provides information arising from urban development such as dynamic and

environmental impacts, but also discriminates complex characteristics of urban landscapes in cities. Due to the useful information in urban change detection that the VIS model can provide, several studies have relied on this fundamental framework for investigating metropolitan ecosystems. Madhavan et al. (2001) used VIS model in evaluating the anatomy and spatial development of metropolitan Bangkok. In this research, Landsat 5-TM imagery was used to produce the land cover types in urban environment over time where changes were recorded. This research emphasizes that remote sensing data is able to be utilized with the VIS in visualizing the changing trends in urban ecosystems. Phinn et al. (2002) and (Lu & Weng 2006) adopt VIS model with the most appropriate image processing methodologies to produce compositions for urban landscapes. They found that VIS can be combined with spectral mixture analysis to produce more accurate results with moderate spatial resolution images. However, they also recognize that impervious surfaces are often overestimated in urbanized regions and underestimated in un-urbanized areas when medium spatial resolution imagery is used.

Due to the complex landscape in urban environment and the mixed pixel problem in medium spatial resolution imagery, the soft classification approach has been developed to achieve a better depiction and accurate estimation of land covers than hard classification approach (Binaghi et al. 1999; Foody & Cox 1994). According to Eastman and Laney (2002), the principle of soft classification lies in the fact that the intercepted radiance is integrated in a solid-state detector at its instantaneous field of view (IFOV). The energy reflecting from a type of land-cover is frequently intercepted by the IFOV at any effective resolution of the detector. As a result, a pixel is able to exhibit

intermediately spectral characteristics of each of the endmember classes. The information derived from sub-pixel estimation will be usually mapped as a fraction of imagery (Shimabukuro, Y, Carvalho & Rudorff 1997) or continuous field (Frizzelle & Moody 2001). However, although sub-pixel analysis is able to be used for quantifying urban impervious areas, it poses some difficulties when working with spectral heterogeneity deriving from urban features (Ji & Jensen 1999).

## **2.6 GIS applications in hydrological modelling**

Hydrological models usually work with multiple spatial data types like topography, soil land use and hydrometeorology. Hydrological models also require watershed partitions into homogeneous units leading to a hydrologic unit derived from those data. Furthermore, one of the crucial components in hydrological modelling is the spatial pattern which can reveal the spatial distribution of hydrological results. Therefore, it is necessary to use GIS, which provides significant tools for analysis of spatial data (Singh & Fiorentino 2013).

### **2.6.1 GIS data**

GIS has the ability to integrate data from multiple sources such as LULC, satellite imagery, boreholes and wells, terrain and surface geology. It allows those data to be used simultaneously to improve our understanding in interactions of the hydrological circle (Ian 2010). Goodchild (1993) argues that six types of data are used in GIS:

i) Irregular point sampling, which includes a set of triples (x, y, z) representing the value of points at a set of locations that are irregular such as precipitation measurement.

ii) Regular point sampling, which includes points arrayed on a rectangular or square grid. An example for this type of sampling is the digital elevation model (DEM).

iii) Contours, which holds a set of lines like digital countour data.

iv) Polygons: each polygon represent an area with the information for that whole area. For example, soil and land use.

v) Cell grid: each cell has a value representing the value of a location within the cell. For example, remote sensing data and rainfall map in raster type.

vi) Triangular Irregular NetWork in which the area is divided into irregular triangles where the verticy ends are pint locations of known maginitude, such as height.

Nowadays, much data used for hydrological models are available for free. Some of the surface data can be derived from the U.S. Geological Survey (USGS) (Landsat imagery and digital elevation models) and FAO (land use and land cover types maps). There are two data types used in GIS, which are vector and raster data. Those data can be used simultaneously for hydrological model calculation by integrating them into the same coordinated system.

### **2.6.2 Hydrological modelling with GIS**

GIS has been integrated into hydrological models for different purposes. Singh and Fiorentino (2013) categorize the integration of GIS and hydrological modelling in stormwater management, watershed modelling, flood prediction and groundwater modelling. Batelaan and De Smedt (2001) integrate GIS in their model name WetSpa for estimating a long-term average spatial distribution of actual evapotranspiration,

groundwater recharge and surface runoff. Fadil et al. (2011) use GIS and the Soil and Water Assessment Tool (SWAT) for stream flow simulation, water balance establishment and monthly volum inflow estimation in Gouregreg basin, Morocco. In the future, with the availability of GIS and remote sensing data sources and the development those technology, hydrological modelling will become more global with a larger distribution and increasing sophistication.

## **2.7 Hydrological model**

### **2.7.1 Hydrological cycle and water balance**

In the natural environment, the occurrence of water circulation is near the surface of the Earth. **Figure 2.1** demonstrates the hydrological cycle. When the solar radiation from the sun reaches to the Earth's surface in general and the ocean in particular, it causes the evaporation of water from oceans. The moisture resulting from the evaporation transports to the atmosphere. In this stage, if favourable conditions are enough, precipitation may be produced. When precipitation occurs, it might be evaporated again to the atmosphere and intercepted by vegetation. A portion of it may infiltrate the soil to become groundwater, be evaporated from the surface of soil and transpired by vegetation. It also can become surface runoff. Groundwater and surface runoff then may travel to lakes and streams and transport back to the ocean.

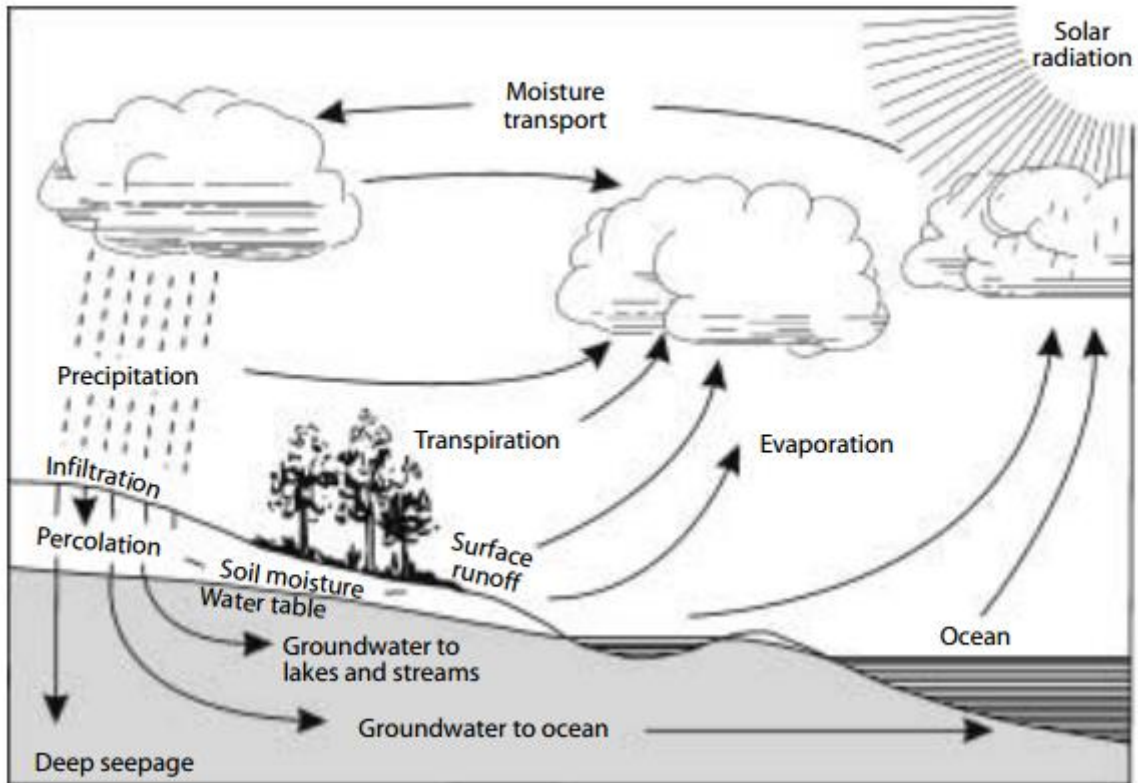


**Figure 2.1.** Hydrological cycle (Zhang, Walker & Dawes 2002)

There are four essential components in the hydrology cycle, which are precipitation, evapotranspiration, surface runoff and groundwater (Zhang, Walker & Dawes 2002). Freeze (1974) explains that the surface runoff component is able to be produced from two mechanisms including saturation and infiltration excess runoff. The infiltration excess runoff is generated by a principle that the different amount between water in and out a system must be equal to the change in the water content of this system. It means, when infiltration or capillary rise to add water to the system, its water content will increase. In contrast, when evapotranspiration or deep drainage cause water decrease, its water content will reduce.

### **2.7.2 Application of WetSpass Model**

As introduced by Batelaan and De Smedt (2001), the WetSpass model was built based on a physical methodology for long-term average and spatial distribution of water balance components including actual evapotranspiration, groundwater recharge and surface runoff. According to those authors, the model was applied in the Grote Nete basin, Belgium for a land-planning project. This study used WetSpass to analyse the influences of land-use changes on groundwater discharge and indicate the necessity of distributed recharge estimation. Pan et al. (2011) evaluate the impact of land-use changes on groundwater recharge under rapid urbanization in Guishui River Basin, China. The WetSpass model was used in this analysis and the results point out that land-use changes resulting from urbanization cause the decrease of early groundwater recharge in the study site. Al Kuisi and El-Naqa (2013) used WetSpass to estimate groundwater recharge for Jafr basin in Jordan. By comparing the results from the WetSpass model with earlier reports of that study area, they concluded that the WetSpass model works well in that study area. Dams et al. (2013) applied sub-pixel imperviousness regression model to produce fraction maps of impervious surfaces from Landsat imagery. This research uses both fixed impervious surface fractions providing by the WetSpass model for urban land-use types and a remote sensing method for estimating imperviousness percentage. The results of their study show that the accuracy of impervious surface fractions is reasonable when deriving from medium resolution remotely sensed imagery. This study also indicates that although there is a similarity of the average spatial changes in water balance constituents caused by urban expansion, WetSpass using land-use data still overestimates the urbanized component in some

smaller urbanized areas and underestimates that component in larger urbanized centres. This leads to the problem that the decrease of groundwater is underestimated in largest urban centres and overestimated in some smaller urban areas.

In general, urbanization and urban expansion cause the increase of impervious surfaces, which are the primary determinant of surface runoff. Hydrological models within a GIS framework are well placed to quantify surface runoff and map its distribution and areas at risk. The WetSpass model can be used to map the spatial distribution of surface runoff. However, this model uses land-use map for its input data and assumes each land use type contains a fixed fractions of vegetation, bare soil, impervious surfaces and open water within a spatial unit. This could be subjective when applied to different study areas due to the different contributions of these materials. Furthermore, mapping impervious surfaces as one input parameter to the hydrological model can be achieved by using remote sensing. Therefore, capturing the variability of land cover types within the pixel could be improve the effectiveness of the WetSpass model.

The next chapter describes the methodology undertaken in this study to estimate surface runoff over the Adelaide Metropolitan areas

## Chapter 3 - Study area and data

### 3.1 The study area

Adelaide is the capital city of South Australia which is located at Latitude  $34^{\circ} 55''$  S and Longitude  $138^{\circ} 35'$  E with an area of approximately  $633.10\text{km}^2$ . The population of Adelaide is around 1.32 million while that of the state of South Australia is approximately 1.7 million in 2015 (ABS 2016). The Western boundary of metropolitan Adelaide is the beach facing Gulf St. Vincent, the South-East is the low lying Mount Lofty Ranges, and the North is the agricultural region shown in **Figure 3.1**. The average elevation of Adelaide is 50 meters above sea level.

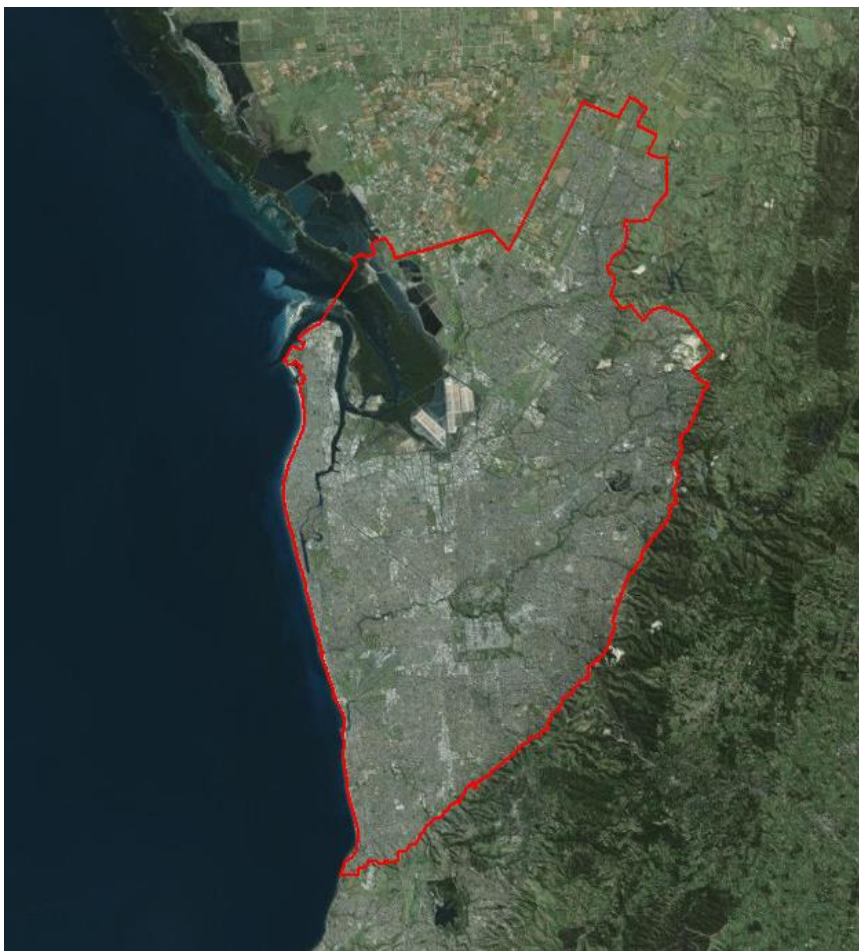


**Figure 3.1.** The study area

According to Wright and Kemp (2016), this city is in a low-lying region. In many cases, stream catchments from higher rural areas often flow through urbanized areas in metropolitan Adelaide. Some parts of the city are also likely affected by overland flow which is not originating from the creek system. The metropolitan Adelaide has several watercourses like Sturt River, River Torrens, Gawler River, Light River and Wakefield River and a number of small creeks enter the plain from the hills such as Adams Creek, Smiths Creeks, Dry Creek, Magazine Creek, Brownhill/Keswick Creek, Waterfall Creek, Christie Creek and Pedler Creek but most dry during summer (Gerges 2006). According to BOM (2016), the annual rainfall of Adelaide is 546.3 mm, the highest temperature is 44.1<sup>0</sup>C on the 2<sup>nd</sup> of January and the lowest temperature was 1.8<sup>0</sup>C on the 20<sup>th</sup> of July 2015.

### **3.1.1 Hydrogeological zones**

According to (Gerges 2006), Adelaide metropolitan area contains six hydrogeological zones (**Figure 3.2**). Zone 1 covers the area of Adelaide hills basement rocks. Zone 2 covers a region lying between Brown Hill Creek and Gulf St. Vincent. Zone 2a connects zone 2 with zone 3. Zone 3 includes a large flat area of the Adelaide plain. Zone 4 covers a large portion of the Golden Grove-Adelaide Embayment and zone 4a is the area between the Eden-Burnside Fault and the extension of the proposed Hope Valley Fault. The upper catchments have an influence on the lower catchments.

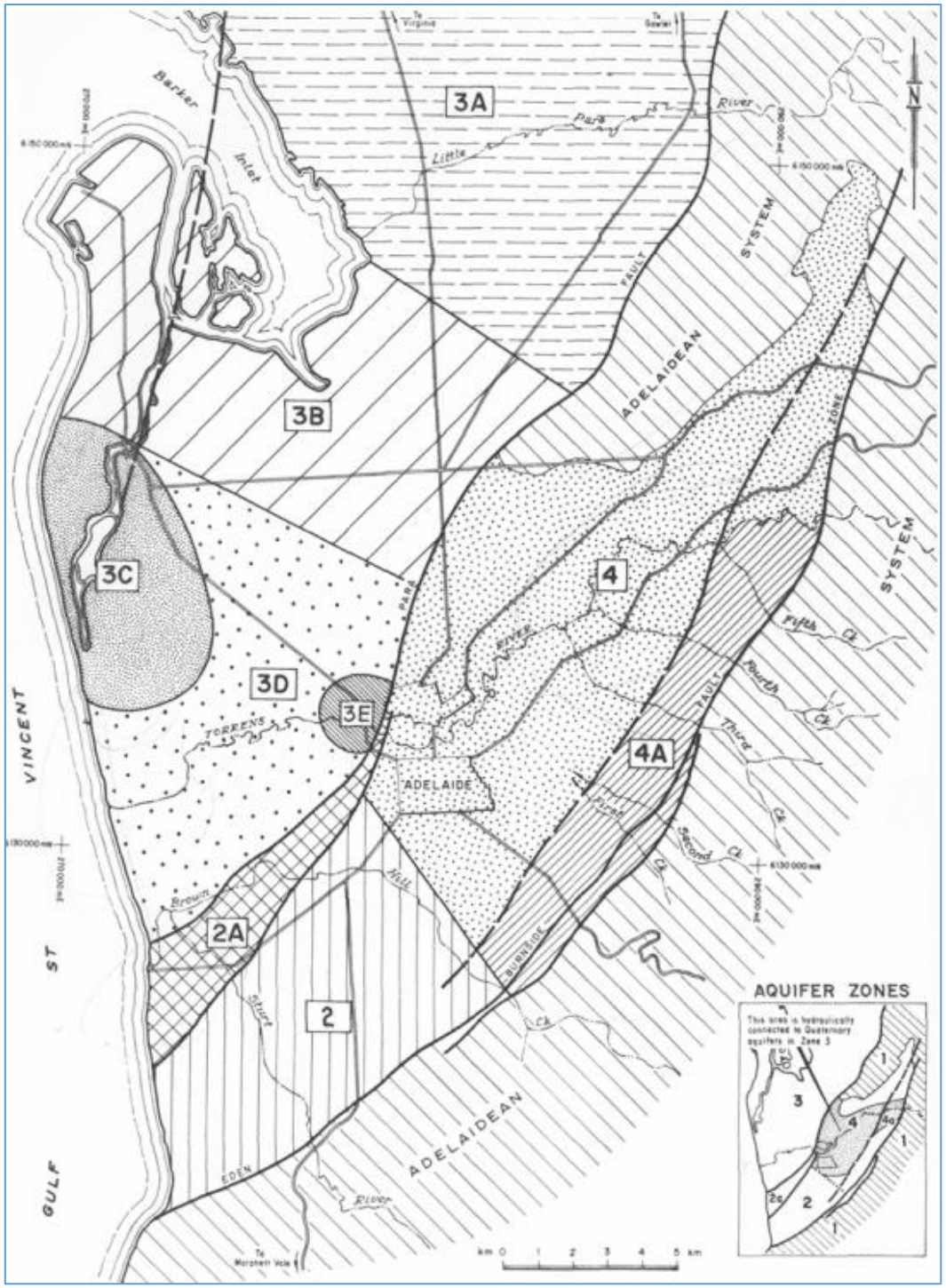


**Figure 3.2.** Hydrogeological zones (Gerges 2006)

**3.1.2 Stormwater in Adelaide**

According to the Parliament of Australia (2015), Adelaide contains much of the old trunk stormwater drainage infrastructure, which was built in the period of 1940s to 1980s. In 2007, the South Australia Government cooperated with the Local Government

Act to produce the plans of storm water management on an agreed catchment basis (Government of South Australia, 2007). This is useful to adapt to the increase of stormwater flows and urban flooding.

### **3.2 Data**

To research surface runoff estimation, spatial data in 2016 was collected for processing and analysing, including Landsat surface reflectance images, soil types, elevation, groundwater depth, climate data such as temperature, rainfall, wind and evapotranspiration. All these data sets were acquired in raster form and were resampled to have the same spatial resolution of 30 m.

#### **3.2.1 Landsat surface reflectance imagery**

Landsat satellite imagery has been provided by the U.S. Geological Survey (USGS) since 1972. Usually, when using this data, users need to pre-process the raw data such for radiometric calibration or atmosphere correction. To alleviate this burden, higher level Landsat satellite products have been distributed by USGS which are called Landsat surface reflectance imagery. These data will contribute science data collection in order to monitor, assess and predict changes of land surface through time and have been calibrated to surface reflectance. USGS has supported Landsat surface reflectance imagery with three versions, which are Landsat 4-5, Landsat 7 and Landsat 8 Surface Reflectance Imagery. In this study, the Landsat 8 Surface Reflectance image acquired on 07 January 2016 was used for analysis. This kind of Landsat satellite data includes elements like original input products, original input metadata, Top of Atmosphere Reflectance, Surface Reflectance and Brightness Temperature. The image collected covers all of the study area at path number 97 and row number 84 (**Figure 3.3**).

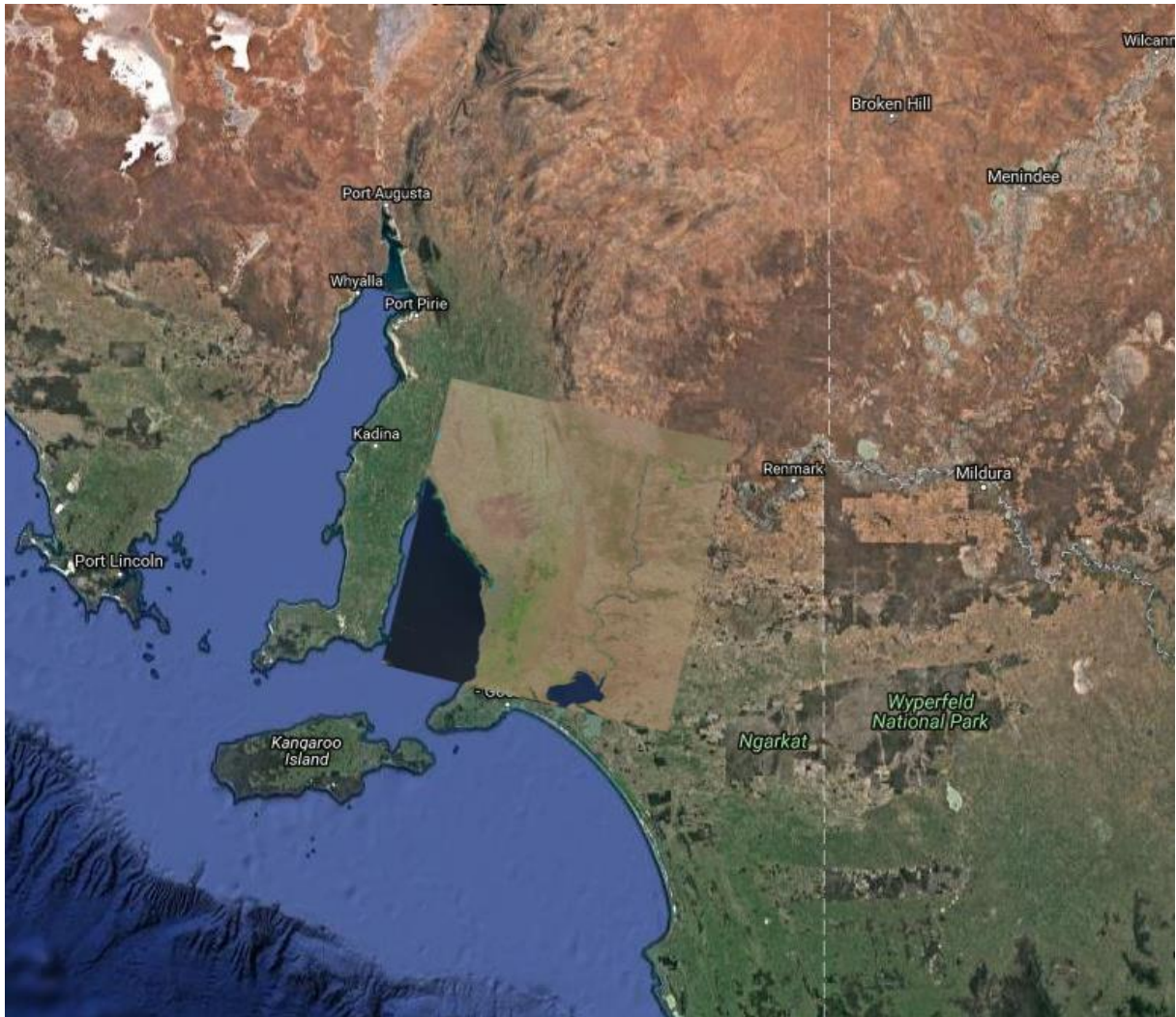


**Figure 3.3.** Landsat scene path 97, row 84

The spatial resolution of this data is 30 meters and is projected to the Universal Transverse Mercator (UTM) coordinate system using the World Geodetic System 1984 (WGS 1984). The Surface Reflectance data represents the reflectance of the Earth's surface. Therefore, the surface reflectance spectra are not affected by atmospheric components. This image, then, was reprojected to The Geocentric Datum of Australia (GDA94) UTM zone 54S. The Landsat 8 surface reflectance image in this study uses 6 spectral bands (band 1, 2, 3, 4, 5, 7) illustrating in **Table 3.1**.

**Table 3.1.** Spectral bands of Landsat 8 imagery used in the research

<b>Bands</b>	<b>Wavelength (micrometers)</b>	<b>Resolution (meters)</b>
Band 1 - Coastal aerosol	0.43 - 0.45	30
Band 2 - Blue	0.45 - 0.51	30
Band 3 - Green	0.53 - 0.59	30
Band 4 - Red	0.64 - 0.67	30
Band 5 - Near Infrared (NIR)	0.85 - 0.88	30
Band 7 – Shortwave Infrared (SWIR) 2	2.11- 2.29	30

### **3.2.2 Land-cover map**

The land-cover map of Adelaide region of 2016 was derived from Landsat 8 Surface Reflectance images by using a supervised classification method. The map includes six classes: Urban, Grass, Road, Bare Soil, Vegetation and Water Body.

### **3.2.3 Land use**

The land use map 2016 was obtained from the Department of Planning, Transport and Infrastructure, South Australia. The original data includes 21 land-use layers: commercial, agriculture, education, food industry, forestry, golf, horticulture, livestock, mine quarry, non-private residential, public institution, recreation, reserve, residential, ret-commercial, river, road, rural residential, utility industry, vacant and vacant residential.

### **3.2.4 Elevation data**

The Digital Elevation Model (DEM) of South Australia has a pixel resolution of 30 m, supplied by the South Australian Government Data Directory was used with a vertical accuracy of 10 meters. The DEM of the metropolitan Adelaide was subset from the larger DEM of South Australia. The elevation of the metropolitan Adelaide ranges from

-4.7 to 300.8 meters above sea level with the highest area is mainly located on the North-East, East and South-East (**Figure 3.4**).

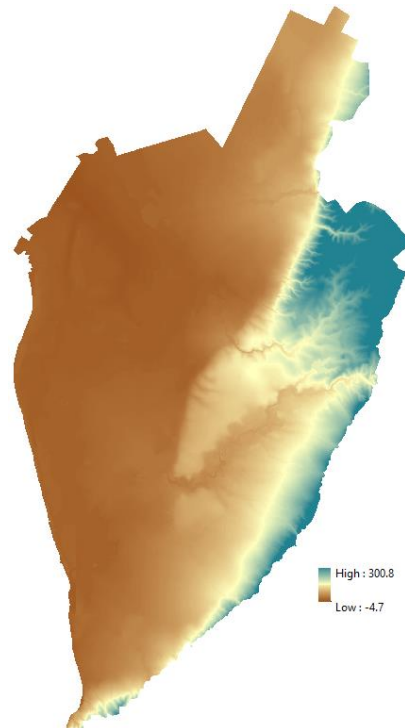


**Figure 3.4.** The DEM of the study area

### 3.2.5 Slope

Slope data was created from the DEM by using the Slope tool in Spatial Analyst, ArcGIS version 10.3.1. Its pixel size is 30 m and its value ranges from 0 to 30.5 degree (**Figure 3.5**). The function of Slope tool assumes that in each cell, the maximum changing rate in value from that cell to its eight surrounding cells is calculated. By calculating this change, the steepest downhill descent from that cell will be identified.

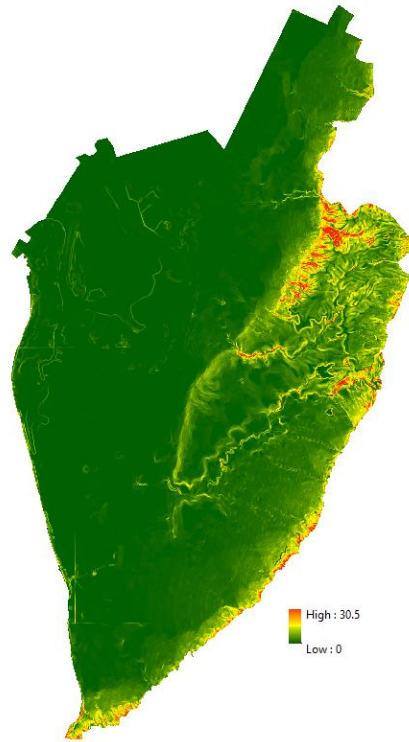


**Figure 3.5.** Slope data of the study area

### **3.2.6 Soil**

Soil data was obtained from the digital version map of the Atlas of Australian soils. The Soil map of the study area was then extracted by using the study boundary and identified based on the soil texture. Soil types of Adelaide region consist of loamy sand, sandy loam, sandy clay loam, clay loam, sandy clay and clay (**Figure 3.6**).

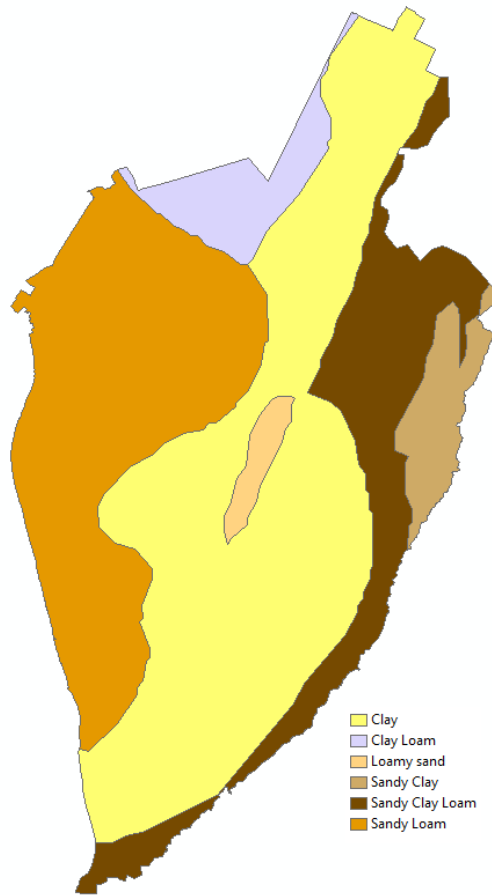


**Figure 3.6.** Soil types in the study area

### 3.2.7 Rainfall map

Rainfall data for 12 months in 2016 was collected from 38 rain gauge observations. Due to missing data for November and December in each rainfall station, the data for those two months were calculated by using the average rainfall of corresponding months of previous years. Kriging interpolator was then used to generate rainfall maps for a 12-month period. The highest average monthly precipitation falls in July, around 134.7 mm and the lowest average monthly precipitation falls in January with approximately 12.7 mm.

### 3.2.8 Temperature

The average temperature data for 12 months in 2016 was collected at 8 temperature observed stations include Edinburgh RAAF, Adelaide Kent Town, Parafield Airport, Adelaide Airport, Mount Banker, Kuitpo Forest Reserve, Noarlunga and Price. The missing data of November and December were observed by calculating the average temperature of previous years. Temperature maps were produced by using Universal Kriging interpolator in ArcGIS. **Table 3.2** shows the average maximum and minimum temperature at 8 temperature observed stations:

**Table 3.2.** Average monthly maximum and minimum temperature at 8 observed stations across the study area in 2016

Month	1	2	3	4	5	6	7	8	9	10	11	12	
T(°C)	Max	14.5	13.3	13.5	11.7	9.5	7.9	7.3	8	9.4	10.7	12.4	13.2
	Min	24.7	22.9	22.7	18.7	16.1	12.7	11.6	12.5	17.2	17.2	20.4	21.8

### 3.2.9 Wind

The mean wind speed values of the period between 1990 and 2010 at 14 wind observed stations across the study region were collected. The wind data was then used to produce the mean wind map for the study area by using the Kriging interpolator. The highest value of mean wind speed is around 21.9 km/h and the lowest value is 11.4 km/h.

### 3.2.10 Potential Evapotranspiration (Pet)

Average Potential Evapotranspiration maps for 12 months over the study area were derived from the Annual Potential Evapotranspiration map of Australia supported by Bureau of Meteorology. The lowest and highest value of average monthly potential evapotranspiration across the study area are illustrated in **Table 3.3**:

**Table 3.3.** Average monthly potential evapotranspiration in Adelaide metropolitan area  
2016

Month		1	2	3	4	5	6	7	8	9	10	11	12
Pet (mm)	Max	176	142	116	72	49	39	44	57	79	118	146	155
	Min	162	132	109	69	43	30	36	51	75	113	135	142

### 3.2.11 Groundwater Depth

To produce groundwater depth raster map, the well data information was collected from the Bureau of Meteorology database. A groundwater depth map of the study area was created using Inverse Distance Weighting (IDW) interpolator with the interpolating value groundwater depth at each well. The highest value of groundwater depth is about 138m and the lowest value is approximately 0.1m (**Figure 3.7**).

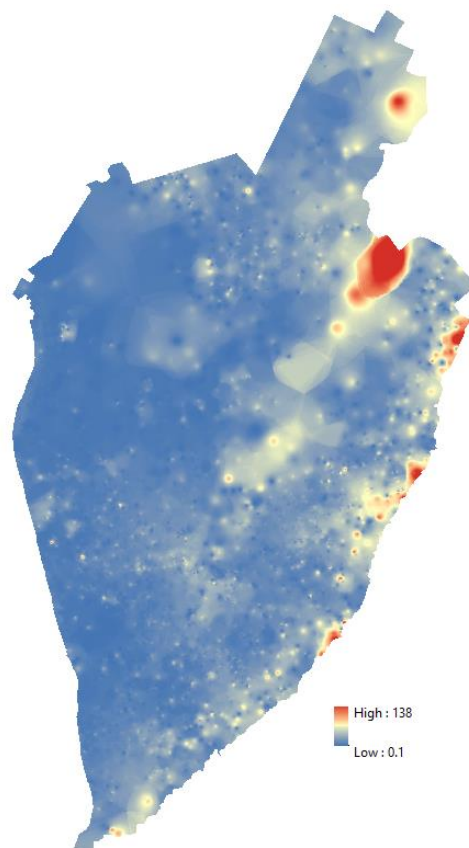


**Figure 3.7.** Groundwater depth across the study area

## **Chapter 4 - Methodology**

### **4.1 Remote sensing method**

#### **4.1.1 Subset image**

A satellite image often contains areas much larger than a particular study area. In this project, the metropolitan Adelaide is only a small part of the Landsat image. Subsetting the study area of this image can eliminate the extraneous data in the image file and increase the speed of the processing because of the smaller data volume in the process. ERDAS Imagine software version 2015 supports the Subset tool for cutting the area of interest. In this study, a Landsat 8 surface reflectance image of Adelaide region in 2016 was used to derive the study area by using Subset tool in ERDAS software with the boundary of the study area.

#### **4.1.2 Supervised classification**

Supervised classification was used to produce the land-cover map over study area. This map was then used to extract water class for the input data of the WetSpas model. As Richards (1999) introduces, a supervised classification technique is often used for deriving land cover information from remotely sensed data. According to the principle of this technique, the spectral domain of bands can be segmented into regions that are able to be associated with ground cover classes of interest. In other words, supervised classification is basically a representation of ground cover type of interest by segmenting multispectral image space and labelling these segments (classes) according land cover types in the field.

The empirical steps applied in the supervised classification technique include:

- i) Decide the land-cover types. In reality, one ground-cover type can reflect different spectrum to the sensor. For example, shallow and deep water, they are the open water. However, that spectral reflectance is different. Therefore, one land-cover type can be an aggregation of sub-ground-cover types.
- ii) Choose the materials of interest which represent pixels for each class. Those pixels are called the training data. The training sets are established through image visual interpretation supported by using Google Earth images.
- iii) Next, those training data are used to estimate the parameters of Maximum Likelihood Classifier algorithm. Those set of parameters are call signatures of the classes.
- iv) Every pixel in the image is then labelled to the corresponding class from the classes determined in the step i) by using the trained classifier.
- v) Produce the thematic map of land-cover types and the tables summarizing class memberships of all pixel in the image.
- vi) When acquiring all of the classes, the sub-ground-cover types representing one type of ground-cover will be recorded to be only one corresponding ground-cover class.
- vii) Finally, the accuracy of the classification map is evaluated by checking with Google Earth images.

In this research, six land-cover classes were used to use in producing land-cover map of the metropolitan Adelaide including urban, grass, infrastructure, bare soil, vegetation and open water.

#### 4.1.3 Spectral Unmixing

According to Keshava and Mustard (2002), Spectral Unmixing Analysis is the process that spectrum of a mixed pixel was decomposed into a constituent spectra set and a correspondingly fractional set. Those constituents of spectra area are known as endmembers (land cover types) and corresponding fractions of these endmembers are named abundances. If calibrated correctly, fractional abundances specify the percentage of each endmember presenting in each pixel location. According to Ghosh et al. (2012), Linear mixture model (LMM) is the most common approach applying in unmixing pixel spectra. In this research, LMM was used to implement spectral unmixing analysis where the results will be input to the WetSpass model to measure the spatial distribution of water balance and surface water runoff. The mathematic expression of LMM is presented as follows:

$$R_i = \sum_{k=1}^n f_k * R_{ik} + \varepsilon_i \quad (\text{Equation 1})$$

In **Equation 1**,  $i$  and  $k$  are the number of spectral bands and endmembers respectively.  $i$  is from 1 to  $m$  and  $k$  ranges from 1 to  $n$ .  $R_i$  is the spectral reflectance at band  $i$  of the pixel;  $f_k$  is the fractional abundance of endmember  $k$  in the pixel;  $R_{ik}$  is the spectral reflectance of endmember  $k$  at wavelength  $i$  of the pixel and  $\varepsilon_i$  is the uncertainty of band  $i$ .

To conduct Spectral Unmixing Analysis, a constrained unmixing condition of  $f_k$  was applied where fraction sum to 1:

$$\begin{cases} \sum_{k=1}^n f_k = 1 \\ 0 \leq f_k \leq 1 \end{cases} \quad (\text{Equation 2})$$

In this research, four endmembers in each Landsat image were investigated which are Vegetation, Impervious Surface, Soil and Open Water (V, I, S and W). Each Landsat image of the study area contains 6 bands. Therefore, the linear relationship among  $R_i$ ,  $f_k$ ,  $R_{ik}$  and  $\varepsilon_i$  in each pixel can be written as a following matrix equation:

Endmembers															
V	I	S	W	Fraction	Error	Image reflectance									
Band 1:	$R_{1V}$	$R_{1I}$	$R_{1S}$	$R_{1W}$	*										
Band 2:	$R_{2V}$	$R_{2I}$	$R_{2S}$	$R_{2W}$				+							
Band 3:	$R_{3V}$	$R_{3I}$	$R_{3S}$	$R_{3W}$						=					
Band 4:	$R_{4V}$	$R_{4I}$	$R_{4S}$	$R_{4W}$								=			
Band 5:	$R_{5V}$	$R_{5I}$	$R_{5S}$	$R_{5W}$										=	
Band 6:	$R_{6V}$	$R_{6I}$	$R_{6S}$	$R_{6W}$											
	$\left[ \begin{matrix} R_{1V} \\ R_{2V} \\ R_{3V} \\ R_{4V} \\ R_{5V} \\ R_{6V} \end{matrix} \right]$	$\left[ \begin{matrix} R_{1I} \\ R_{2I} \\ R_{3I} \\ R_{4I} \\ R_{5I} \\ R_{6I} \end{matrix} \right]$	$\left[ \begin{matrix} R_{1S} \\ R_{2S} \\ R_{3S} \\ R_{4S} \\ R_{5S} \\ R_{6S} \end{matrix} \right]$	$\left[ \begin{matrix} R_{1W} \\ R_{2W} \\ R_{3W} \\ R_{4W} \\ R_{5W} \\ R_{6W} \end{matrix} \right]$	$\left[ \begin{matrix} F_V \\ F_I \\ F_S \\ F_W \end{matrix} \right]$	$\left[ \begin{matrix} \varepsilon_1 \\ \varepsilon_2 \\ \varepsilon_3 \\ \varepsilon_4 \\ \varepsilon_5 \\ \varepsilon_6 \end{matrix} \right]$	$\left[ \begin{matrix} R_1 \\ R_2 \\ R_3 \\ R_4 \\ R_5 \\ R_6 \end{matrix} \right]$								

The Root Mean Square of error (RMSE) is used to evaluate the fitness of the model. It was computed by the following formula:

$$\text{RMSE} = \sqrt{\frac{\sum_1^m \varepsilon_i^2}{m}} \quad (\text{Equation 3})$$

As Mather and Koch (1999) state, smaller RMSE indicates better fit of the sum of fractions, while higher RMSE shows poor fit of the model. Consequently, the indication and the fractional images of the endmembers are better when the RMSE image is lower.

The spectra of the known endmember are required in linear spectral unmixing analysis. Those spectra can be acquired directly from the image by measurement or obtained from a spectral library (Yang, C, Everitt & Du 2010). In this study, three broad endmember classes were directly selected from the image, which are vegetation, impervious surface and bare-soil. Open water was derived directly from land-cover map. The spectral unmixing analysis was conducted by the ENVI software version 5.0. The region of interest of vegetation, impervious area and bare-soil was created. When selecting endmembers on the image, Google Earth imagery was used as an extra source to ensure achieving suitable endmembers.

## **4.2 GIS method**

### **4.2.1 Kriging**

Kriging is a statistical technique that calculates the weight in the weighted moving average formula. It assumes that with points closer together, they are spatially correlated and their correlation reduces when the distance between the sample points increases. The points close together have higher probability of having similar values. This is measured by using an experimental semi-variogram (Borough & McDonnell 1998, p. 155). There are different types of Kriging such as Ordinary Kriging, Universal Kriging and Co-Kriging. In this research, the Universal Kriging was used to produce rainfall, temperature, groundwater depth and wind speed maps. Universal Kriging is the interpolation method used in the presence of external trends. It assumes that there are some underlying deterministic trends present in its structure (Borough & McDonnell 1998, p. 149; Kalkhan 2011, p. 87).

#### 4.2.2 Inverse Distance Weighting (IDW)

In this study, IDW was used to generate the groundwater depth map by using known groundwater depth values measured from wells across the Adelaide metropolitan area. In the IDW operation, cell values are determined by using a linearly weighted combination of a point group from the sample points (**Figure 4.1**). An inverse distance function is used for the weight. Therefore, the resulting interpolated surface will have the influence of a locally dependent variable (in this case, the locally dependent variable is the groundwater depth values of nearest wells of the interpolated wells). The assumption of IDW is that influence of the variable being interpolated between points (in this case groundwater depth) reduces due to the increase of distance from its sampled location (ArcGIS ESRI 2016). In **Figure 4.1**, the values of red points which have a local influence on the yellow point are used to interpolate the value of yellow point.

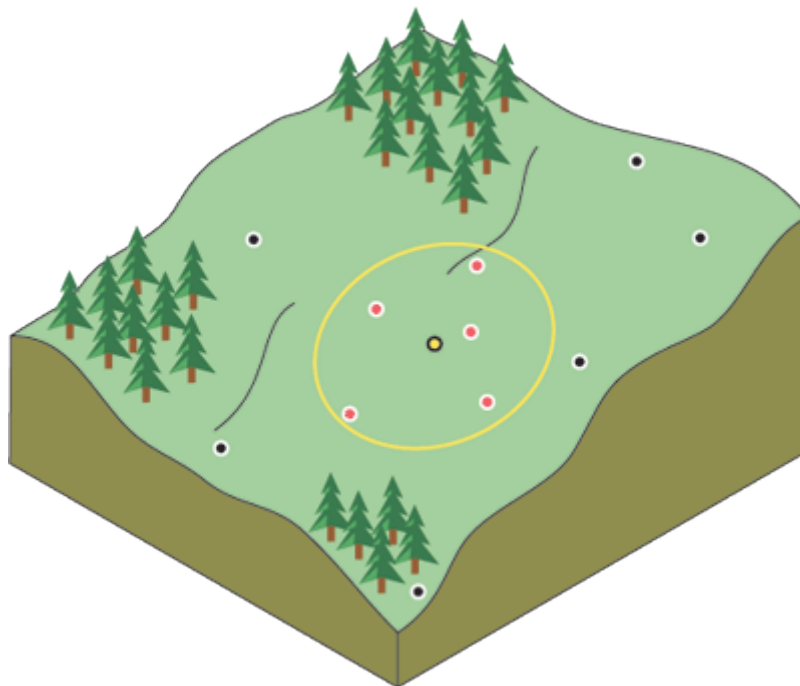


**Figure 4.1.** Neighbourhood (red points) for selected point (yellow point) (ArcGIS ESRI, 2016)

### 4.2.3 Recoding the data

The 2016 land-use map contains 21 layers as described in the section 3.2.3. These classes were minimized to 12 land-use classes by aggregation in order to conform to the requirements of the WetSpass model. Google Earth imagery, along with land-cover map derived from the supervised classification, were used to help guide the aggregation of land-use classes using the Raster Calculator tool in ArcGIS. Then, those land-use types were used to determine the corresponding land-use types provided by WetSpass model to obtain corresponding codes (**Table 4.1**). By the same way, soil types of Adelaide were assigned to the corresponding soil types provided by the model with soil codes including loamy sand (code = 2), sandy loam (code = 3), sandy clay loam (code = 7), clay loam (code = 9), sandy clay (code = 10) and clay (code = 12). Those codes of land use and soil types were used for calculation in WetSpass model. All assigning data work were implemented in ArcGIS software.

**Table 4.1.** Derived land-use types of the study area and corresponding information in the WetSpass model

Code	LUSE_TYPE	Runoff vegetation	VEG AREA	BARE AREA	IMP AREA	Land use
2	Orchard	forest	0.2	0.8	0	Agriculture
5	Grassland	grass	1	0	0	Golf
8	Coniferous forest	forest	0.9	0.1	0	Reserve
11	Dunes	bare soil	0.3	0.7	0	Vacant
13	Water	open water	0	0	0	River
16	Residential	grass	0.5	0	0.5	Horticulture and residential
17	Military areas	grass	0.6	0.1	0.3	Education and public institute
18	Commerce and services	grass	0.3	0	0.7	Commercial and road
19	Industry	grass	0.4	0	0.6	Industry
20	Mining	bare soil	0	1	0	Mine quarry
21	Infrastructure	grass	0.6	0.1	0.3	Livestock Recreation and rural residential
22	Harbour	grass	0.6	0.1	0.3	

### **4.3 The WetSpass model**

WetSpass model was developed by Batelaan and De Smedt (2001). The model is used for estimating the spatial distribution of groundwater recharge, evapotranspiration and surface runoff by investigating physical and empirical relationships in a long-term. The WetSpass model requires input data in raster form including land-use/land cover, elevation, soil texture, slope and climate data like rainfall, potential evapotranspiration, wind and temperature. According to Batelaan and De Smedt (2001), in order to address the heterogeneous nature of LULC, four sub-pixel proportions or fractions of LULC are defined at the raster cell (pixel) scale, including vegetated cover, impervious surfaces, bare soil and open water fractions. In this research, the more recent WetSpass-M software model, developed by Abdollahi et al. (2015), which is the raster-based monthly water balance was used to calculate surface runoff.

#### **4.3.1 Model concept**

The performance of WetSpass is based on the computation of water balance at the pixel level. water balances is obtained by summing the independent water balances for vegetation, impervious surfaces bare soil and open water proportions/fractions of of each raster cell. Therefore, the total water balance of a given area is computed by summing the water balance of each raster cell. Notably, the WetSpass model provides predefined/default proportions of land cover fractions for specific LULC types, but according to Batelaan and De Smedt (2001), the calculated water balance for each raster cell can be improved if actual land cover (LC) fractions can be derived. In this case the proportion of each land cover fraction can more realistically vary within each land use type.

### 4.3.2 Calculating water balance for each raster cell

The total water balance is calculated by using water balance components of vegetation, impervious surface, bare-soil and open-water. This calculation is demonstrated as below:

$$ET_{\text{raster}} = a_v ET_v + a_s E_s + a_o E_o + a_i E_i \quad (\text{Equation 4})$$

$$S_{\text{raster}} = a_v S_v + a_s S_s + a_o S_o + a_i S_i \quad (\text{Equation 5})$$

$$R_{\text{raster}} = a_v R_v + a_s R_s + a_o R_o + a_i R_i \quad (\text{Equation 6})$$

where  $ET_{\text{raster}}$  is the total evapotranspiration,  $S_{\text{raster}}$  is surface runoff and  $R_{\text{raster}}$  is groundwater recharge of a raster cell;  $a_v$ ,  $a_s$ ,  $a_o$  and  $a_i$  are the vegetation, bare-soil, open-water and impervious area component correspondingly;  $E$  is evapotranspiration (Batelaan and De Smedt, 2001)

### 4.3.3 Calculating Surface runoff

According to Abdollahi et al. (2015), a rational approach applying for a monthly time-step is used in calculating surface runoff volume in WetSpa-M. This approach uses two coefficients and it is demonstrated in **Equation 7**:

$$SR_m = C_{sr} C_h (P_m - I_m) \quad (\text{Equation 7})$$

Where  $P_m$  is monthly precipitation (mm/month),  $I_m$  is monthly interception (mm/month),  $SR_m$  is the monthly surface runoff (mm/month) and  $C_{sr}$  is the coefficient of actual surface runoff,  $C_h$  is the coefficient representing the condition of soil moisture as Bahremand et al. (2007) indicated and it is calculated using the following formula:

$$C_h = \left( \frac{\theta_s}{\theta_{sat}} \right)^b \quad \text{(Equation 8)}$$

Where  $\theta_s$  is the soil moisture content of the cell ( $m^3/m^3$ ),  $\theta_{sat}$  is soil porosity ( $m^3/m^3$ ) and  $b$  is an exponent which represents the influence of rainfall intensity. If  $b$  is equal to one, the relation between soil moisture and its condition ( $C_h$ ) is assumed to be linear. According to Bahremand et al. (2007), when temporal changes of discharge are used, the optimal value can be obtained with conducting calibration. By integrating  $C_h$  in **Equation 7**, over-estimation of surface runoff is avoided in semi-arid areas having low soil moisture and high potential evapotranspiration. When soil moisture data at monthly time-step is scarce, the evaporative efficiency ratio (introduced by Creutzfeldt et al. 2010; Xingnan & Göran 1997) is integrated into the adapted approach of Turc (1955) at monthly level:

$$C_h = \frac{P_m}{LP(P_m^\alpha + ET_m^\alpha)^{\frac{1}{\alpha}}} \quad \text{if } ET_m > P_m \quad \text{(Equation 9)}$$

$$C_h = 1 \quad \text{if } ET_m \leq P_m$$

Where  $ET_m$  is monthly potential evapotranspiration (mm/month),  $LP$  is a calibration parameter used to reduce the potential evapotranspiration.

In this study, the WetSpass model was used to run using both the predefined and ‘actual’ fractions of LULC to produce the results of surface runoff over study area. These results of these two methods were then compared to evaluate the reliability of the result.

As detailed above, remote sensing methods including subset imagery, supervised classification and Spectral Unmixing Analysis and GIS methods such as Kriging and

IDW were used to generate the input data for the WetSpass model. The calculation of surface runoff in the recent version of WetSpass model (WetSpass-M) was introduced. Importantly, both the land-use with predefined/default LC proportions and the LC proportions/fractions derived from the SMA approach were input to the WetSpass model to calculate two optional results of surface runoff maps.

## Chapter 5 - Results

This chapter presents the result of the land-use map derived from minimizing information; the fractional maps obtaining from Spectral Unmixing method and the monthly and annual distribution of surface runoff. The full view of the results is illustrated in the **Appendices** section of this thesis.

### 5.1 Land use map

After combining the original land-use map obtained from the Department of Planning, Transport and Infrastructure, South Australia and the land-cover map derived from supervised classification process, the resulting new land-use map is presented in **Figure 5.1**.

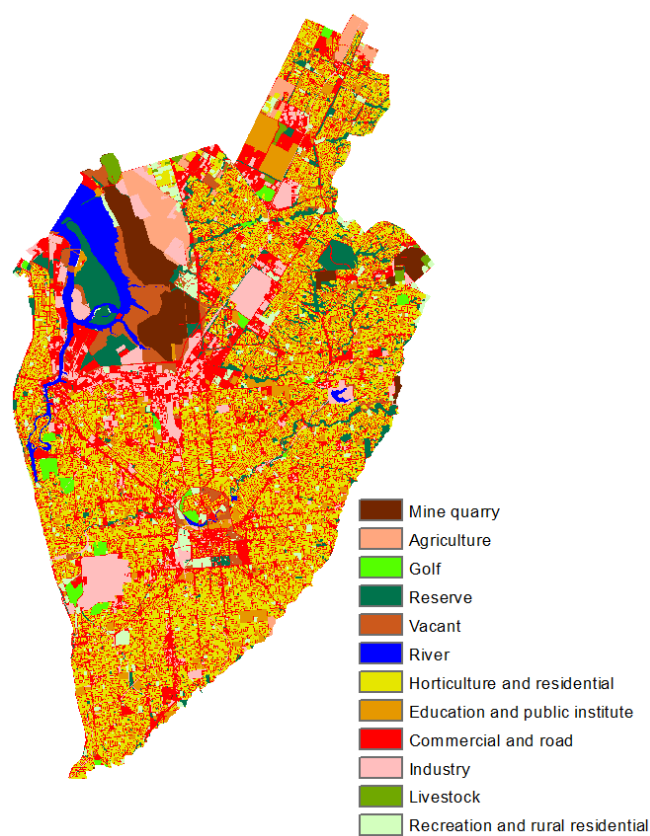


**Figure 5.1.** Land-use map of the study area

The study area consists of 12 land-use types (**Table 5.1**) with the predomination of horticulture and residential (22,916.80 ha). Commercial and road rank as the second largest with the area of 17,033.00 ha where this kind of land-cover type also contains the highest abundance of impervious surfaces. Reserve and industry have a similar area, which is 4105.26 and 4854.78 ha respectively. Livestock and Golf have the smallest area with 305.37 and 732.33 ha respectively.

**Table 5.1.** Land use types in the study area

<b>Code</b>	<b>Name</b>	<b>Area (hectare)</b>
21	Livestock	305.37
5	Golf	732.33
2	Agriculture	1411.29
13	River	1902.69
22	Recreation and rural residential	2164.41
20	Mine quarry	2244.15
11	Vacant	2400.12
17	Education and public institute	3217.14
8	Reserve	4105.26
19	Industry	4854.78
18	Commercial and road	17033.00
16	Horticulture and residential	22916.80
<b>Total</b>		<b>63287.34</b>

## 5.2 Spectral Unmixing Analysis results

### 5.2.1 Endmember selection

Three endmember signatures of vegetation, impervious surface and bare soil within the study area were collected. The spectral reflectance of those endmembers are plotted in **Figure 5.2**. Vegetation exhibits strong reflectance in the near-infrared wavelengths (0.85 - 0.88 micrometers) and low reflectance in the blue and red wavelengths (0.45 - 0.51 and 0.64 - 0.67 micrometers respectively), while soil reflects strongly in the

middle-infrared wavelength (0.85 - 0.88). Impervious surfaces have different reflectances due to highly mixed materials between and within a pixel.

and a low reflectance at band 1 and 2 while soil significantly responds at band 6 and impervious surfaces have different reflectance due to highly mixed materials within a pixel.

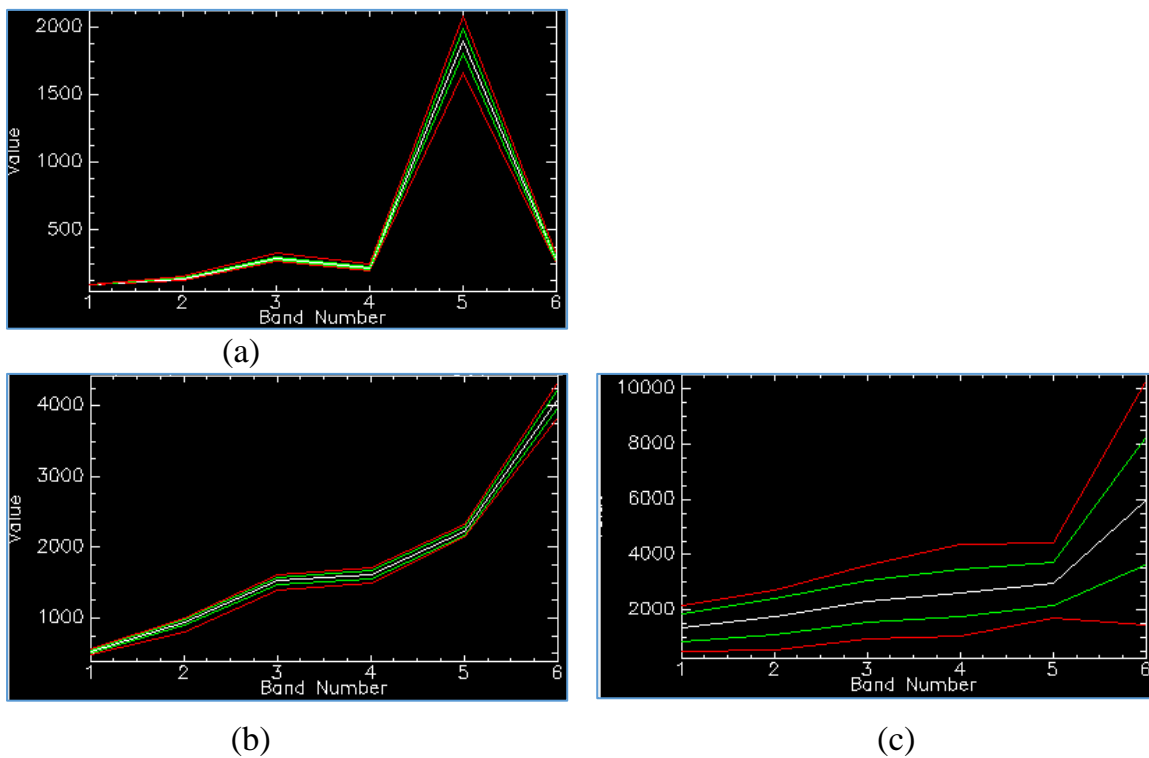


**Figure 5.2.** Spectral reflectance of vegetation (a), bare soil (b) and impervious surface (c) at six spectral bands of the image

The statistics of each endmember signature are shown in **Table 5.2**, **Table 5.3** and **Table 5.4** bellows. The mean reflectance values of impervious surfaces in all six bands are significantly greater than those of the two other endmembers.

**Table 5.2.** Statistics of selected vegetation endmember

<b>Basic Stats</b>	<b>Min</b>	<b>Max</b>	<b>Mean</b>	<b>Standard deviation</b>
Band 1	93	101	95.05634	2.254439
Band 2	127	156	138.6338	6.370108
Band 3	265	331	290.6479	11.49546
Band 4	195	248	219.2535	9.845548
Band 5	1664	2076	1898.662	88.58345
Band 6	244	315	275.7183	16.89225

**Table 5.3.** Statistics of selected bare soil endmember

<b>Basic Stats</b>	<b>Min</b>	<b>Max</b>	<b>Mean</b>	<b>Standard deviation</b>
Band 1	483	566	533.5926	21.37982
Band 2	815	1006	949.3333	39.12603
Band 3	1396	1608	1526.519	50.58684
Band 4	1488	1710	1622.185	57.91707
Band 5	2146	2321	2225.296	51.23537
Band 6	3842	4330	4110.037	124.4275

**Table 5.4.** Statistics of selected impervious surface endmember

<b>Basic Stats</b>	<b>Min</b>	<b>Max</b>	<b>Mean</b>	<b>Standard deviation</b>
Band 1	486	2150	1352.696	494.32
Band 2	552	2699	1771.652	645.9223
Band 3	957	3611	2318.261	763.7657
Band 4	1044	4352	2629.174	846.8335
Band 5	1710	4433	2946.522	797.0649
Band 6	1444	10286	5984.174	2290.501

### 5.2.2 Endmember abundance maps

The fractional abundance maps of vegetation, bare soil and impervious surfaces resulting from Spectral Unmixing analysis and map of open water derived from the supervised classification are presented in **Figure 5.3**. As can be seen from these maps, the highest abundance of vegetation is concentrated on the East and North-East of Torrens Island. Furthermore, a higher proportion of vegetation also appears along rivers and creeks, and where there are parks and recreation areas. Vegetation does not appear in the open water area, some bare soil areas and some commercial regions. In terms of

bare soil, the highest abundance of bare soil can be found surrounding the Salt Crystallisation Pans located in the Northern Greenfields Wetlands, Southern Tramway museum, around Golden Grove Recyclers and in the North of the study area where agricultural land is predominant. Lower abundance of bare soil can be found in the Southern parts of the study area where the residential density is higher. The open water 'abundance' map was directly obtained from the land cover map, derived from the supervised classification result. It is presented here as a binary map of open water and non-water areas with 'abundance' values of 1 (100%) and 0 (0%) respectively. Impervious fractions are abundant and at their highest in the CBD of Adelaide city and industrial and commercial areas like supermarkets and car parks. The proportion of impervious surfaces gradually decreases from the CBD to the Northern metropolitan areas where the density of residential allotments is lower and conversion to some agricultural land areas exists.

In general, the proportions of vegetation, impervious surfaces, bare soil and open water within every pixel sum closely to 1. Therefore, if the abundance of any one of those endmembers is 1 (or 100%), the fractions of other endmembers elsewhere are zero.

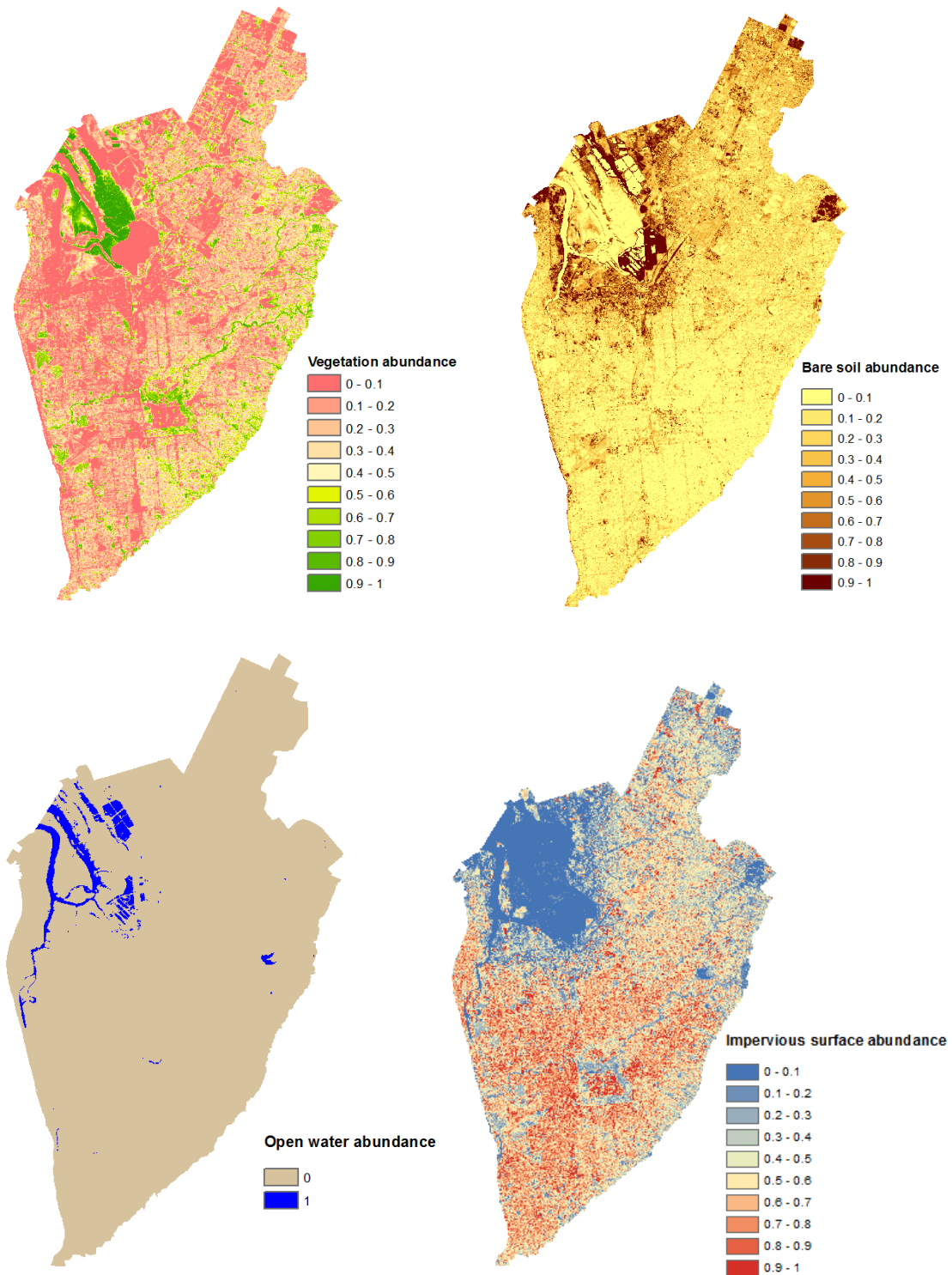


**Figure 5.3.** Fractional maps of vegetation, bare soil, open water and impervious surfaces

**Table 5.5** shows the mean abundance value for each of the four endmembers over study area. As can be seen, the mean proportion of impervious surfaces at 0.459 is

significantly higher than for vegetation and bare soil at 0.263 and 0.247 respectively.

The proportion of open water is lowest at 0.031.

**Table 5.5.** Mean values of vegetation, bare soil, open water and impervious surfaces over the study area

	Vegetation	Bare soil	Open water	Impervious surfaces
Mean value	0.263	0.247	0.031	0.459

### 5.3 Spatial distribution of surface runoff

The spatial distribution of surface runoff was derived from the WetSpass model by conducting two methods, using the land cover map and fractional maps as the input data separately. The results were calculated monthly and annually.

#### 5.3.1 Monthly surface runoff patterns

**Figure 5.4.** Spatial patterns of surface runoff 2016 over metropolitan Adelaide using land-use types and **Figure 5.5** bellows show the spatial distribution of surface runoff across the study area during 12 months in 2016. . Overall, the amount of surface runoff resulting from the WetSpass model using the land cover fractions derived directly from the Landsat image using Spectral Unmixing is greater than that of the land-use map with predetermined/default fractions of vegetation, bare soil, impervious surfaces and open water.

As the results from using the land-use map with default land cover fractions in WetSpass (**Figure 5.4**) show, the lowest amount of surface runoff falls in April when the monthly precipitation for this month is lowest; almost no runoff anywhere irrespective of the LULC type. The mean value of rainfall in April for every pixel is

around 8.3 mm and the mean value of surface runoff in that month is approximately 1.5 mm for each cell within the study area. In contrast, the highest surface runoff volume is in July at appropriately 40.7 mm for each pixel when the precipitation is highest (mean rainfall value of every pixel within the study area is nearly 102.5 mm). The mean amount of runoff in May is second highest, about 33.9 mm per pixel. The mean surface runoff in February and October are similar, about 6.3 and 6.2 mm perpixel respectively. In every month, most of the higher values of surface runoff are in open water area and in some areas in inland where the rainfall intensity is higher.

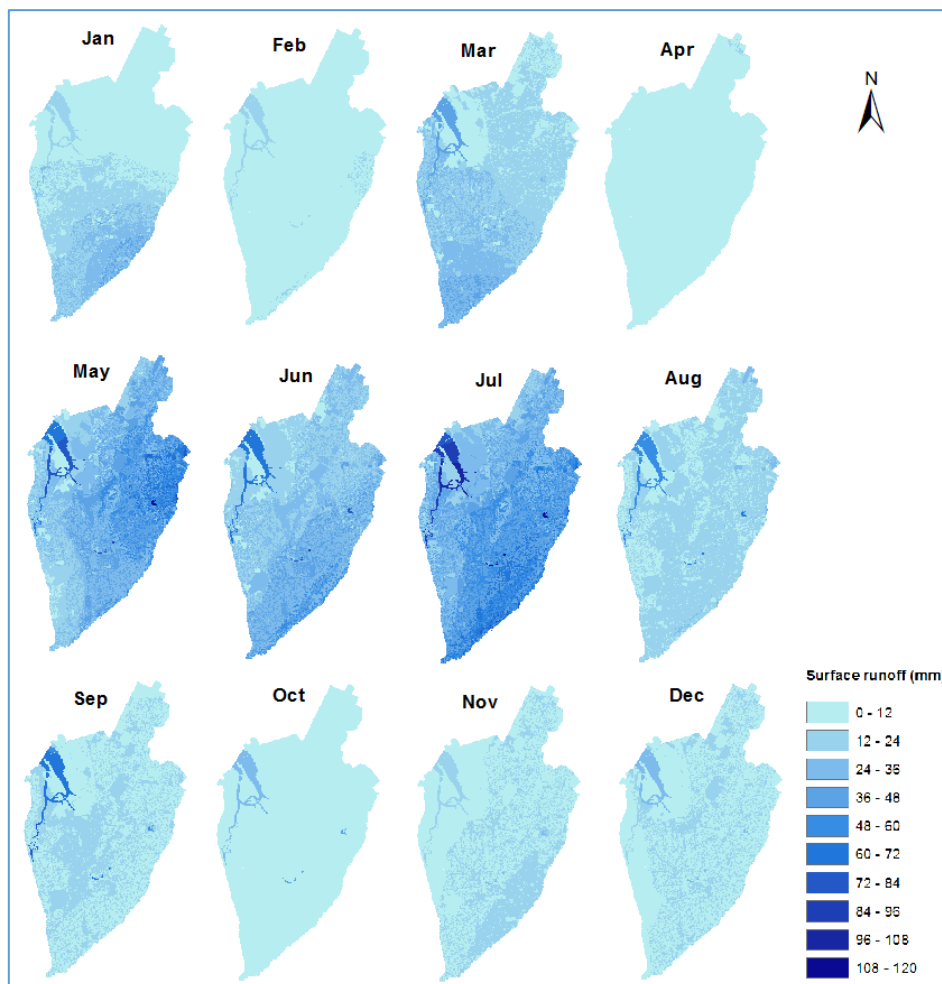


**Figure 5.4.** Spatial patterns of surface runoff 2016 over metropolitan Adelaide using land-use types and default land cover fractions

As the results using Spectral Unmixing Analysis derived land cover fraction of vegetation, bare soil, impervious surfaces and open water in WetSpass (**Figure 5.5**) show, the highest and lowest amount of surface runoff are in July and April at 47.8 and 2.0 mm respectively. Except for the result in April, which has the lowest amount of surface runoff, it can be seen that the higher volume of surface runoff can be found in the open water areas and in areas of high density impervious surfaces such as commercial and residential areas. These results also reveal lower surface runoff value in the vegetated areas surrounding the CBD; contrasting with the higher surface runoff within the CBD.

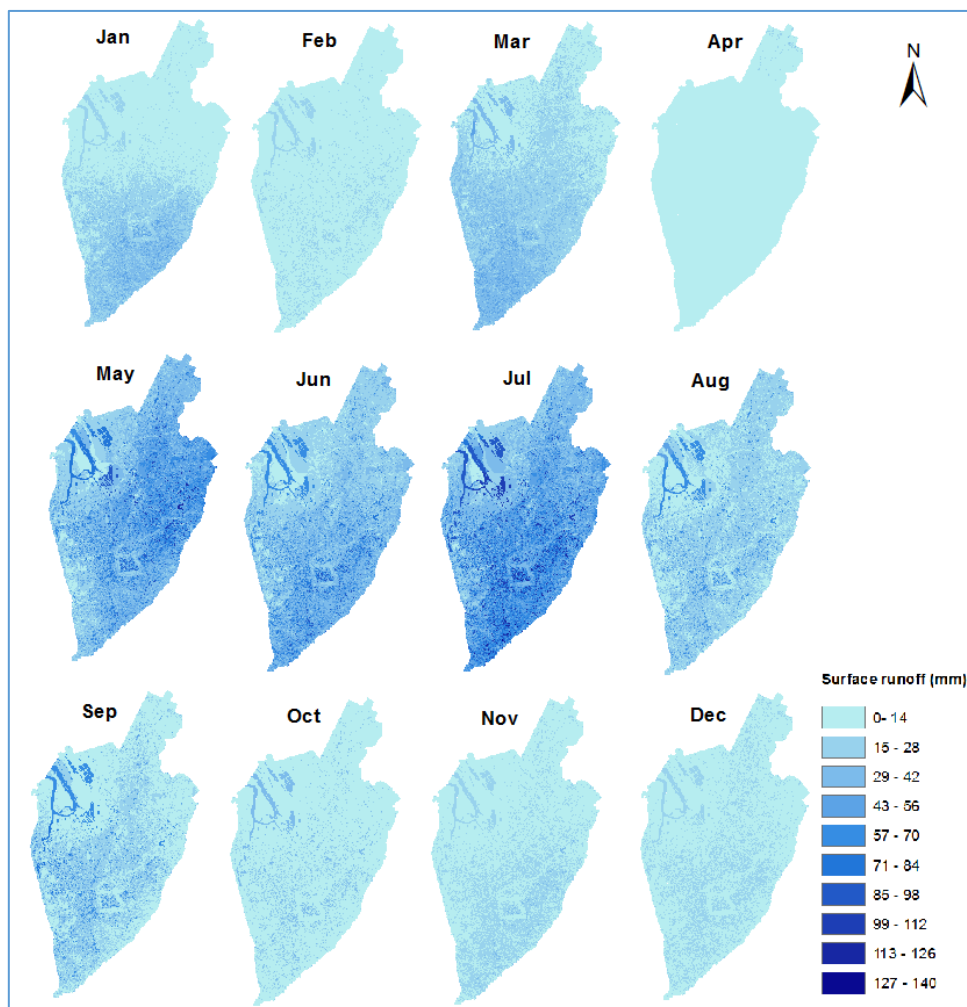


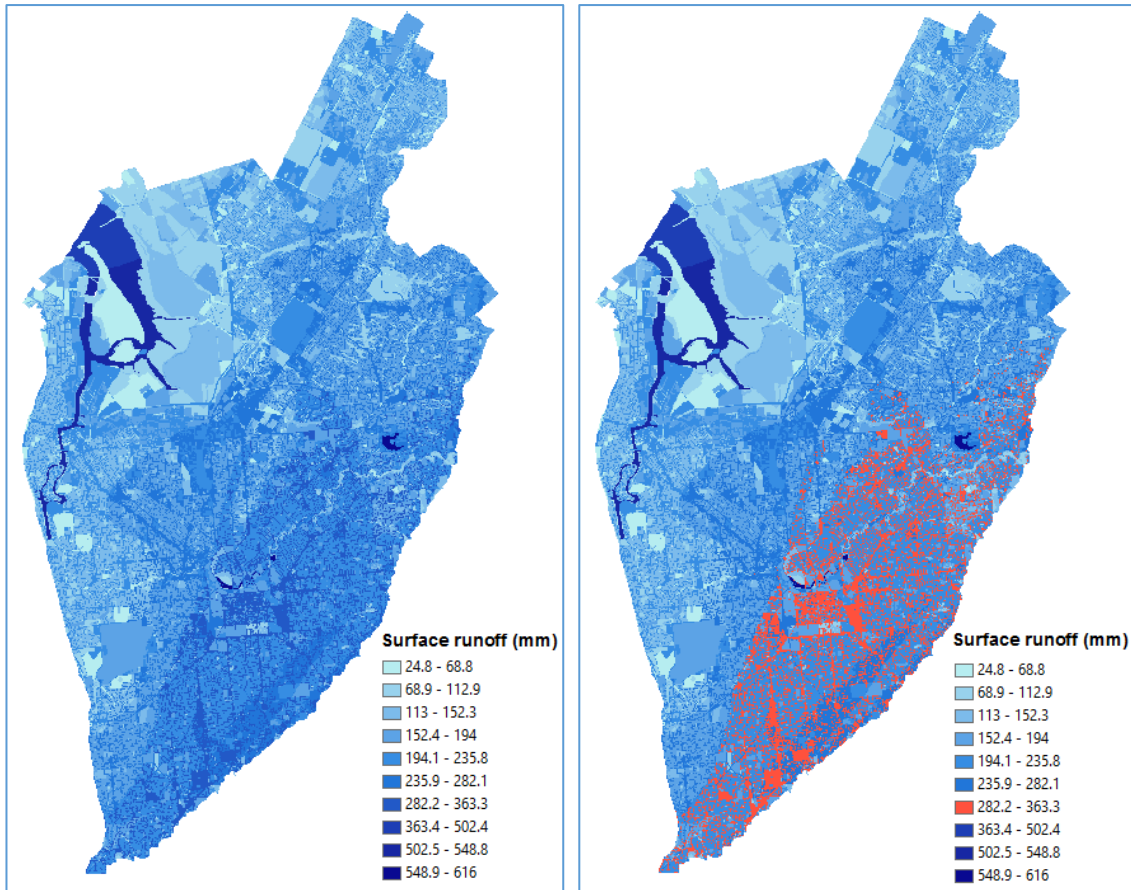
**Figure 5.5.** Monthly spatial distribution of surface runoff 2016 using fractional maps derived from Spectral Unmixing

### 5.3.2 Annual surface runoff distribution

The annual surface runoff maps from these two methods were derived by summing the monthly surface runoff maps over the 12-month period for 2016.

#### a. WetSpss using land-use map and default land cover fractions

**Figure 5.6** – (a) presents the spatial distribution of annual surface runoff across the study area. As the figure shows, the highest amount of annual surface runoff is associated with the open water areas like Torren River, Hope Valley Reservoir and Port Adelaide River. These annual surface runoff values range between 363.4 and 616 mm per pixel. In the inland areas, the highest annual surface runoff value is allocated in the red colour and is found in South-Eastern Adelaide (**Figure 5.6** – b). These red coloured areas have annual surface runoff ranging between 282.2 and 363.3 mm per pixel and are typically roads and commercial areas as defined in the land-use map. Three categories of the highest annual surface runoff value in **Figure 5.6** are located in open water areas and they are not marked.



(a)

(b)

**Figure 5.6.** Annual surface runoff 2016 using land-use map: a) – The whole study area; b) – The highest annual runoff in the inland area (red colour)

The two lowest surface runoff value ranges are from 24.8 to 68.8 mm and 68.9 to 112.9 mm and are mainly distributed in the Northern part of the study area. The two lowest value ranges (yellow and green colour) mostly lie over open reserves, vacant lands, public institutions, golf courses and along some rivers and creeks where vegetation and grass are predominant (**Figure 5.7**).

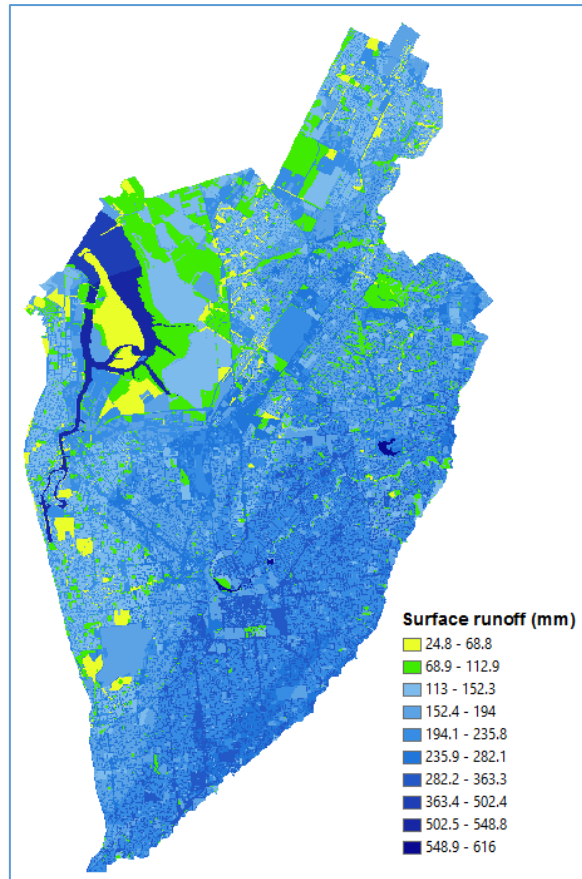


**Figure 5.7.** The lowest values of annual surface runoff

**b. WetSpss using fractional maps from Spectral Unmixing Analysis**

**Figure 5.8** illustrates the spatial distribution (**Figure 5.8 – a**) and the highest annual surface runoff values over study area (distinguished by the red colour in **Figure 5.8 – b**). Overall, the higher values of surface runoff are distributed fairly evenly over the congested areas where impervious surfaces are predominant, such as buildings and commercial areas. The lower values are mainly found in the Northern areas and in some parts of the South-West of the study area.

In **Figure 5.8 – b**, the highest range of surface runoff values range between 558.2 and 687.6 mm per pixel and are represented with the colour red. The majority are found in some parts of the Torrens River and over the Hope Valley Reservoir and the high density buildings and houses such as in the CBD, the area near the Maid Hotel,

surrounding the Good Guys at Mile End and PETstock Melrose Park along with Harvey Norman at Gepps Cross.

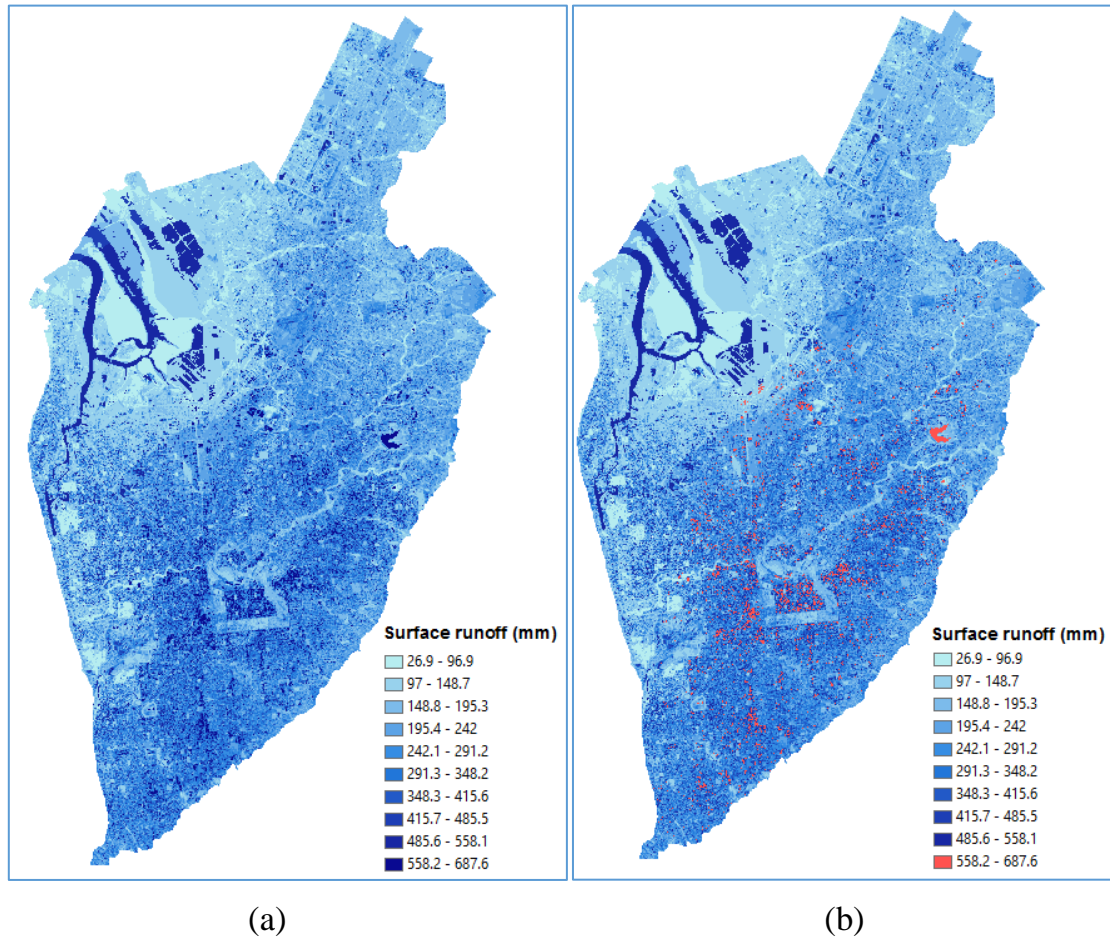


**Figure 5.8.** Annual surface runoff 2016 using fractional maps of Spectral Unmixing Analysis: a) – For the whole study area, b) – The highest annual runoff across the study area

**Figure 5.9** presents the two lowest ranges of annual runoff surface values resulting from using the fractional maps (portrayed in the yellow and green colour). These values are primarily distributed over the areas where vegetation and grass are predominant. Those areas include most of Torrens Island, the large area of vegetation surrounding Torrens Island, some areas in the Northern and South-Eastern Adelaide, along rivers and creeks and in recreation areas.

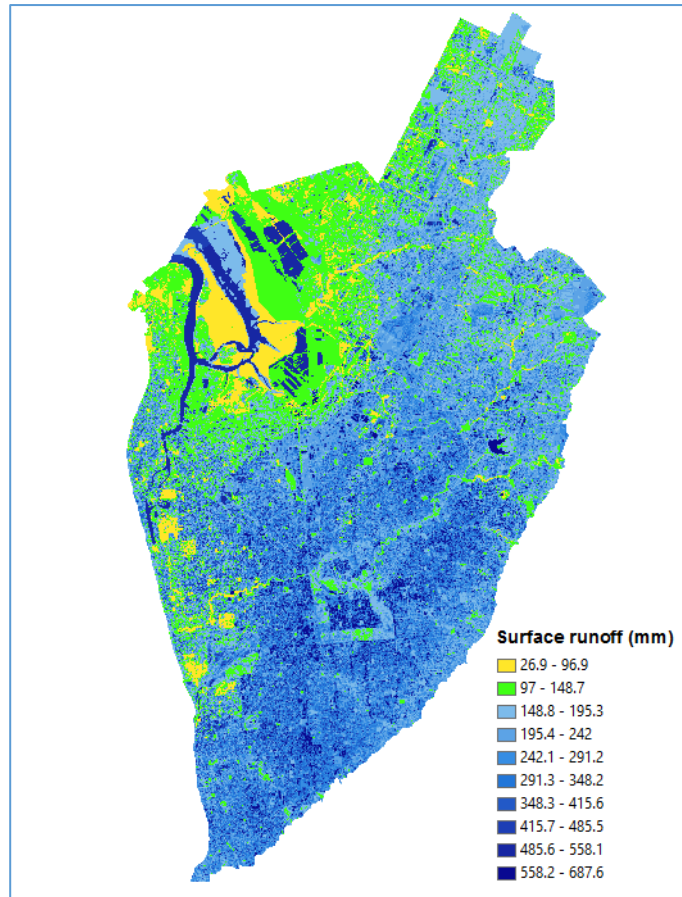


**Figure 5.9.** The lowest values of annual surface runoff resulting from Spectral Unmixing Analysis

## Chapter 6 - Discussion

### 6.1 General findings

#### 6.1.1 Spectral Unmixing Analysis

To assess the reliability of fractional maps resulting from Spectral Unmixing Analysis, the Zonal Statistics as Table tool in ArcGIS was used to statistically test the land cover fractions of vegetation, bare soil, impervious surfaces and open water against known impervious land-use types. The two land-use categories of ‘Commercial and Road’ and ‘Industry’ were chosen for this test as they are dominated by impervious surface areas such as buildings, car parks and roads. Therefore, it is expected that the mean value of impervious surface fractions within these two land-use categories would be greater than that of vegetation and bare soil.

After implementing the Zonal Statistics tool in ArcGIS, the mean values of endmembers covering each land-use category were calculated and are illustrated in **Figure 6.1**.

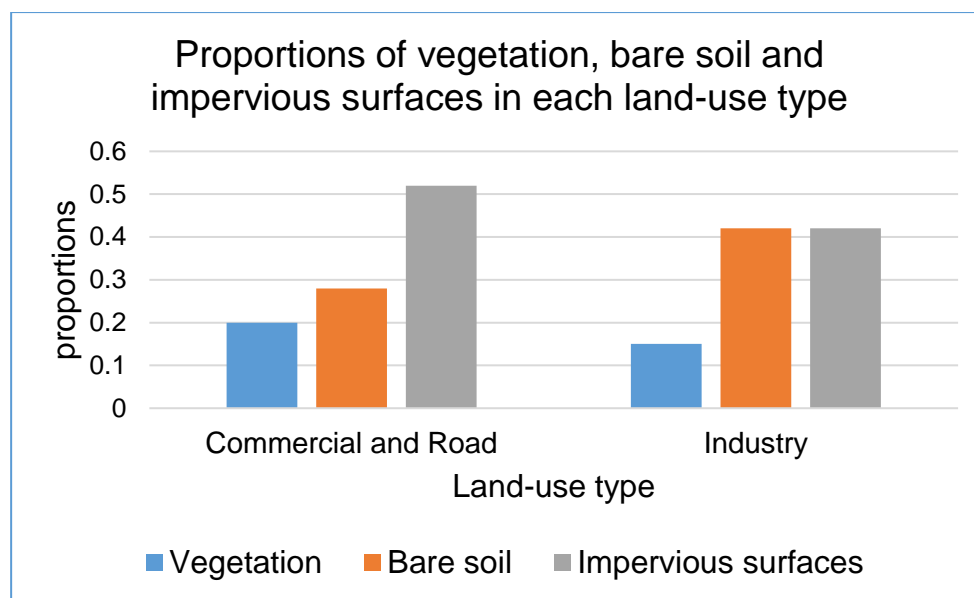


**Figure 6.1.** Proportions of vegetation, bare soil and impervious surfaces covering each ‘impervious’ land-use type

As **Figure 6.1** shows, impervious surfaces predominates the Commercial and Road category with the proportion of 52%. The contributions of vegetation and bare soil are much lower at 20% and 28% respectively. In terms of the Industry category, impervious surfaces and bare soil equally contribute to land-cover proportion with 42% for each; the percentage of vegetation in this category is 15%. Thus, the results of Spectral Unmixing Analysis are reasonable and reliable.

### 6.1.2 Spatial distribution Surface runoff volume

Surface runoff distribution is affected considerably by soil types in both the WetSpass predifined/default land cover fractions and Spectral Unmixing derved land cover fractions. It can be clearly recognized in the months that have higher rainfall, such as in May, June, July, and August, that loamy sand seems to allow more infiltration according to the WetSpass model, while clay likely prevents more water running into the ground (**Figure 6.2**).

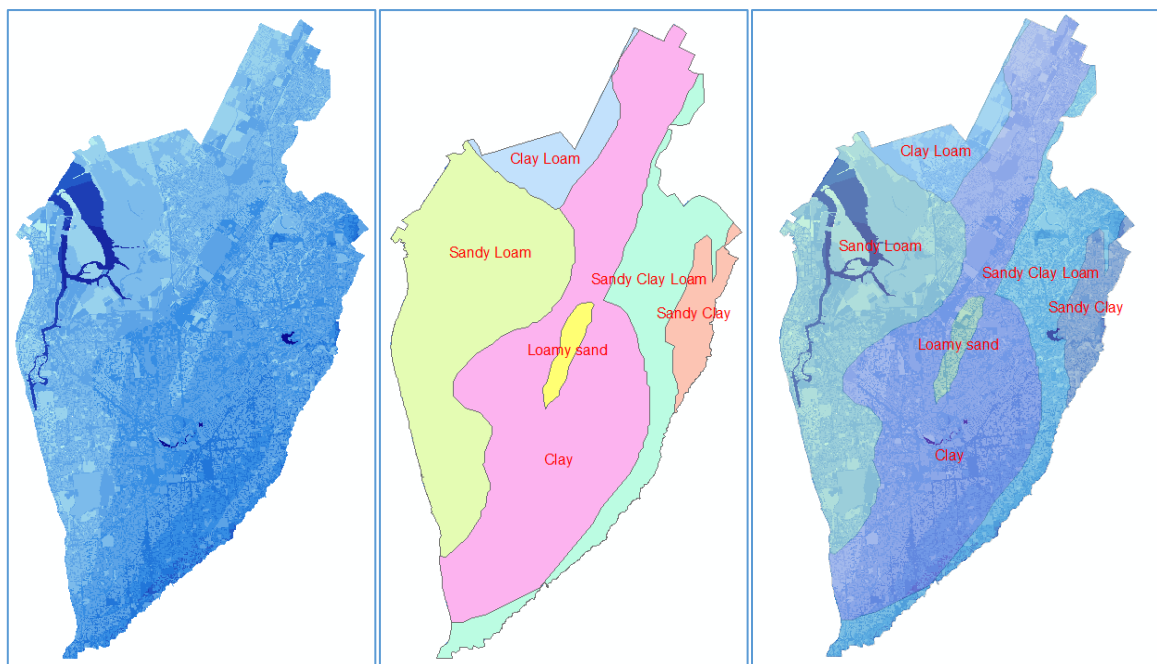


**Figure 6.2.** Surface runoff distribution and soil types in the study area in July, 2016 (surface runoff map + soil map + overlaid soil map and surface runoff map)

The WetSpass model uses land-use data in calculating the water balance, including surface runoff. This land-use data contains different discrete land-use categories separated by boundaries where each category defines a unique land use type (Koomen et al. 2011). However, one discrete land-use type might hold many different land cover types. For example, an educational land-use category may contain buildings, paths, lakes and vegetated areas. These features or land cover types may occupy different proportions within the area of a single pixel location and thus is a mixed pixel. A single land-use category usually consists of many contiguous pixels consisting of both pure and mixed pixels of varying land cover types. The WetSpass model typically assumes fixed proportions of land cover fractions for each land-use type. This means that every pixel within the boundary of a land-use type has the same proportions of vegetation, bare soil, impervious surfaces and open water. This only partly addresses the mixed pixel problem. As the results show, the surface runoff volume of each pixel in one land-use type, where it has the same soil type and rainfall, tends to have the same value.

For instance, in **Figure 6.3** an area near the Adelaide Airport is defined as a golf course in the land-use map with the area being around 85 hectares. It consists of approximately 944 pixels (the cell size is 30 meters). The fractions that WetSpass assigns for each pixel in that land-use type are 1, 0, 0 and 0 for vegetation (it is grass in this case), bare soil, impervious surfaces and water respectively. This means that only vegetation covers the golf course. However, in reality, each pixel in that area includes a different mixed proportion of vegetation, soil and impervious surface. Therefore, using the land-use map with default LC fractions in WetSpass may overestimate or underestimate surface

runoff volumes in some areas, especially in areas having mixed pixels with different contributions of vegetation, bare soil, impervious surfaces and open water.

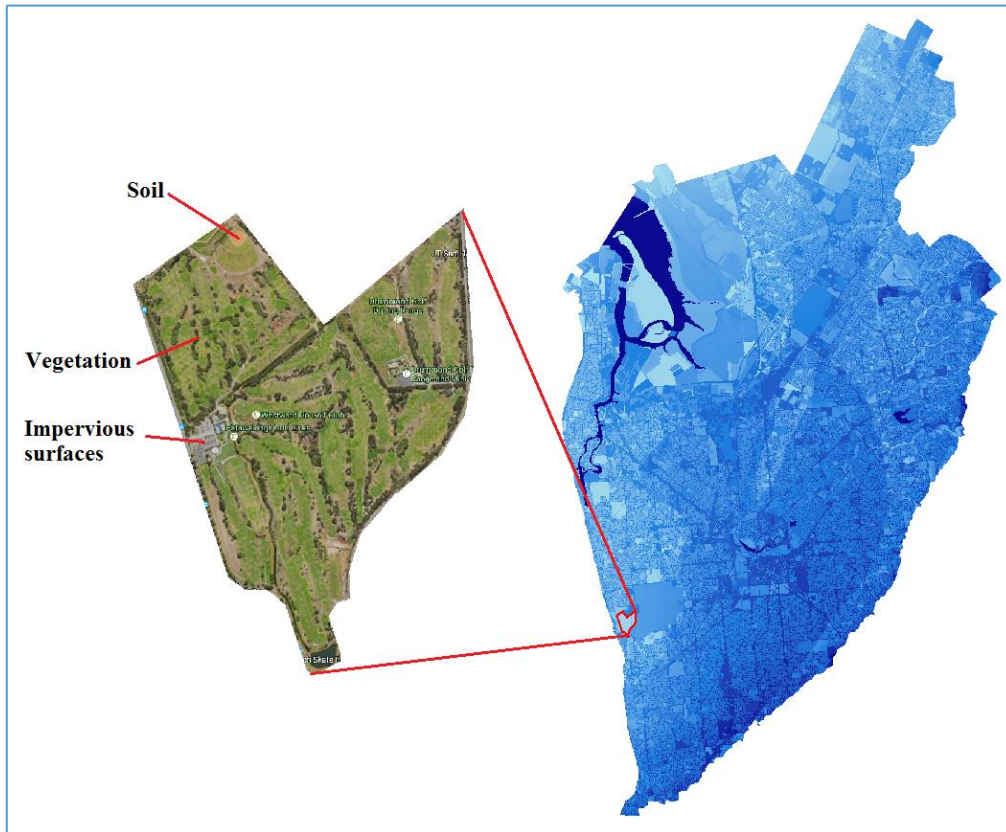


**Figure 6.3.** Mixed vegetation, soil and impervious surfaces in one land-use type

Conversely, Spectral Unmixing Analysis attempts to map the actual variation in land cover composition in each pixel. Because the mapped proportions of vegetation, bare soil, impervious surface and open water contributing to one pixel varies based on the reflectance spectrum of each endmember, the surface runoff volume also varies within each land-use category and across the study area. The approach lends itself to both homogeneous and heterogeneous landscapes. In homogeneous areas the surface runoff volumes are similar where the fractional proportions of land cover types are consistent with adjacent pixels derived from consistently similar spectral reflectance curves between pixels (Small 2004). Therefore, the proportions of vegetation, bare soil,

impervious surfaces and open water are similar to adjacent pixels in those areas (**Figure 6.4**).

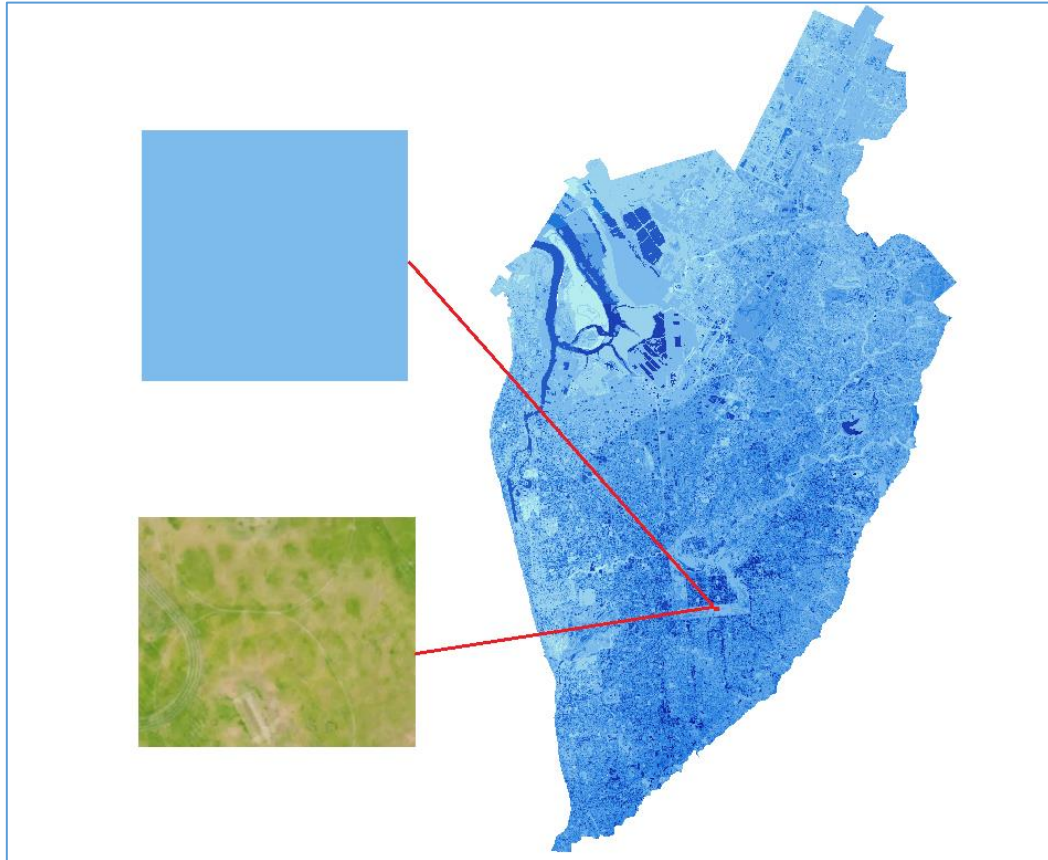


**Figure 6.4.** Homogeneous pixels in surface runoff map of July and the corresponding land cover

On the other hand, in heterogeneous areas like residential and commercial areas, the fractional contributions of the four endmembers in each adjacent pixel varies based on the complexity of these areas (Shimabukuro, YE & Smith 1991). Consequently, the amount of estimated surface runoff for each pixel will also vary (**Figure 6.5**).

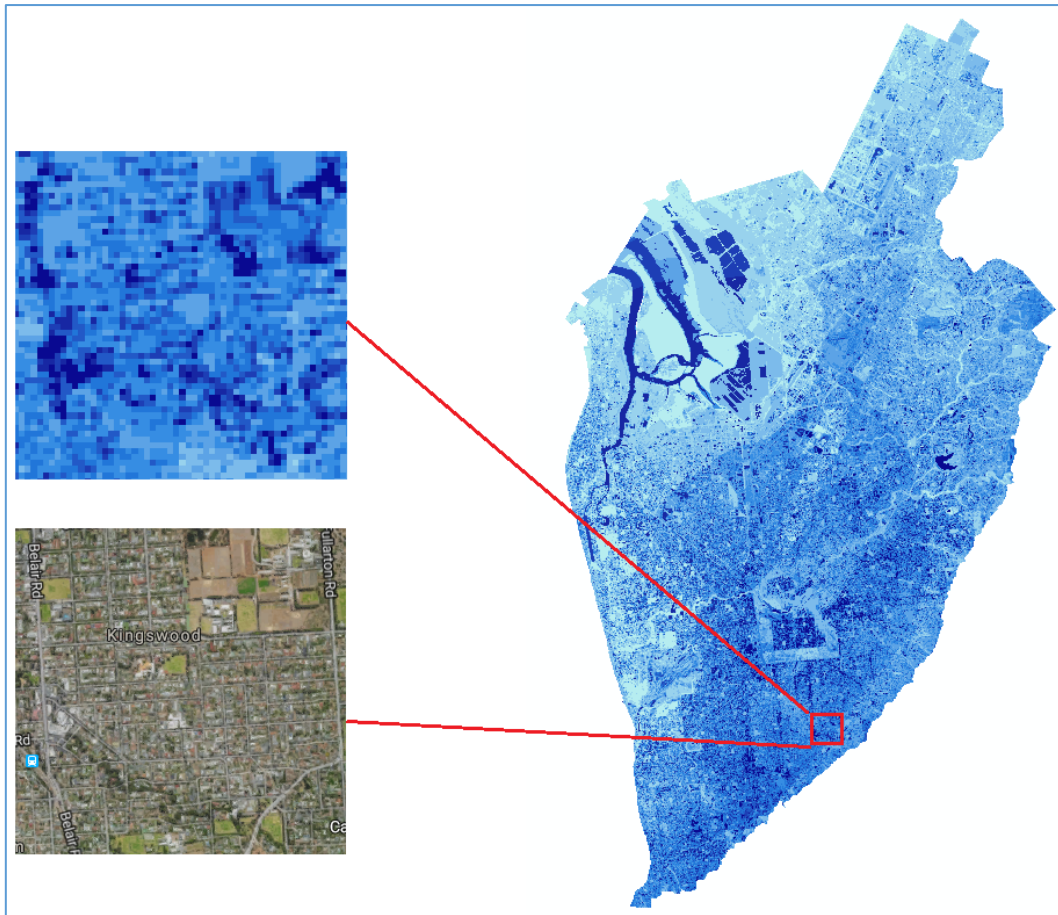


**Figure 6.5.** Heterogeneous pixels in surface runoff map of July and the corresponding land cover

### 6.1.3 Comparisons between two approaches

#### a. At the monthly level

As the discussion above shows, the results of WetSpass model using the land-use map with predefined/default LC fractions is likely to under or overestimate surface runoff volumes in some areas where complex and differing land cover types exist. In contrast, the results when using Spectral Unmixing of land cover types with the WetSpass model are likely to be more reliable. By using a Spectral Unmixing approach, the variation of vegetated, bare soil, impervious and open water proportions across heterogeneous areas in the urban environment can be better estimated as they are more indicative of the actual land cover composition in these areas. Therefore, the ‘classic’ remote sensing

problem of mixed pixels is solved. However, to gain more confidence in determining which approach is more accurate requires validation of the results by using statistics and comparing the results with previous studies in the Adelaide metropolitan area.

**Figure 6.6** shows the surface runoff results in a heterogeneous area of two approaches used in this research. WetSpass using land-use data underestimates the amount of surface runoff while Spectral Unmixing method coupled with WetSpass can determine the difference in surface runoff volume in this area. This is reasonable because Spectral Unmixing method not only can solve mixed pixel problems, but also reveals the relation between impervious surfaces and the amount of surface runoff as reviewed in the section **Impervious surfaces and surface runoff**. Because the study area is the urban environment and it is predominated by the mixture of land cover types, the results of monthly surface runoff derived from WetSpass using land-use data are probably underestimated.

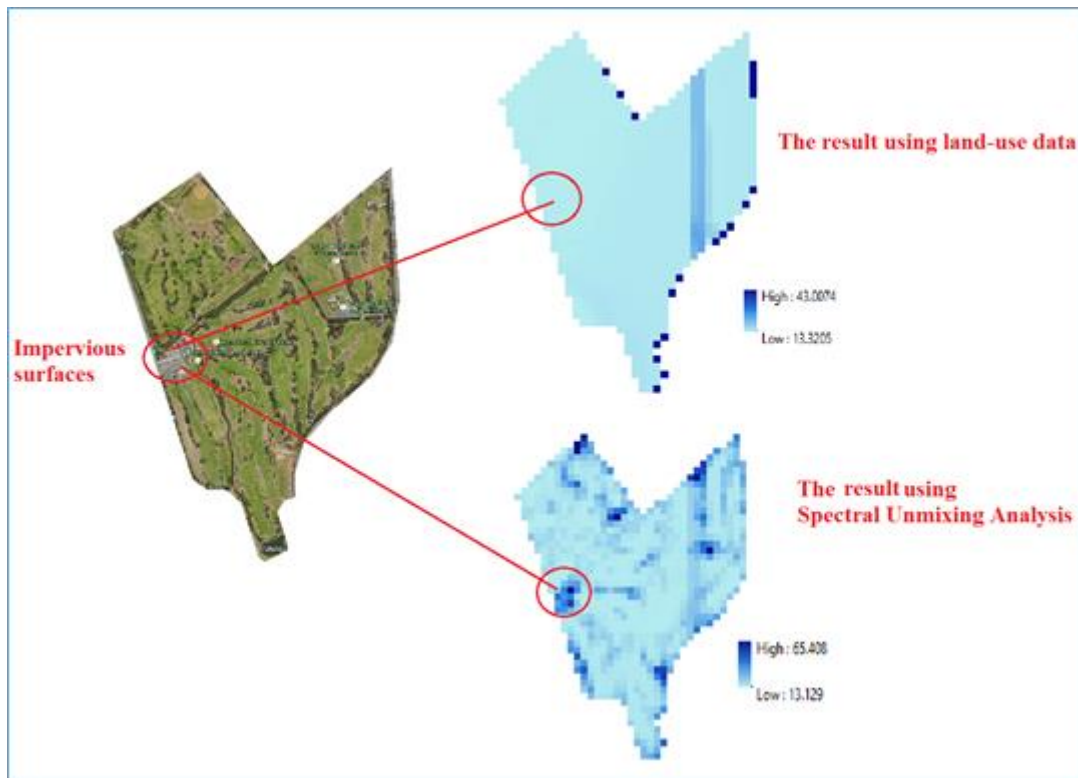


**Figure 6.6.** Surface runoff in a heterogeneous area resulting from the two approaches

In addition, **Figure 6.7** shows the mean value of monthly surface runoff in 2016 using both the default and derived LC fractions in the WetSpss model. Overall, the surface runoff volume in every month from the Spectral Unmixing approach is higher than that using the land-use map and default LC fractions in the WetSpss model. The highest difference between the mean surface runoff values of the two methods are in the months having the highest rainfall intensity such as in May, June and July.

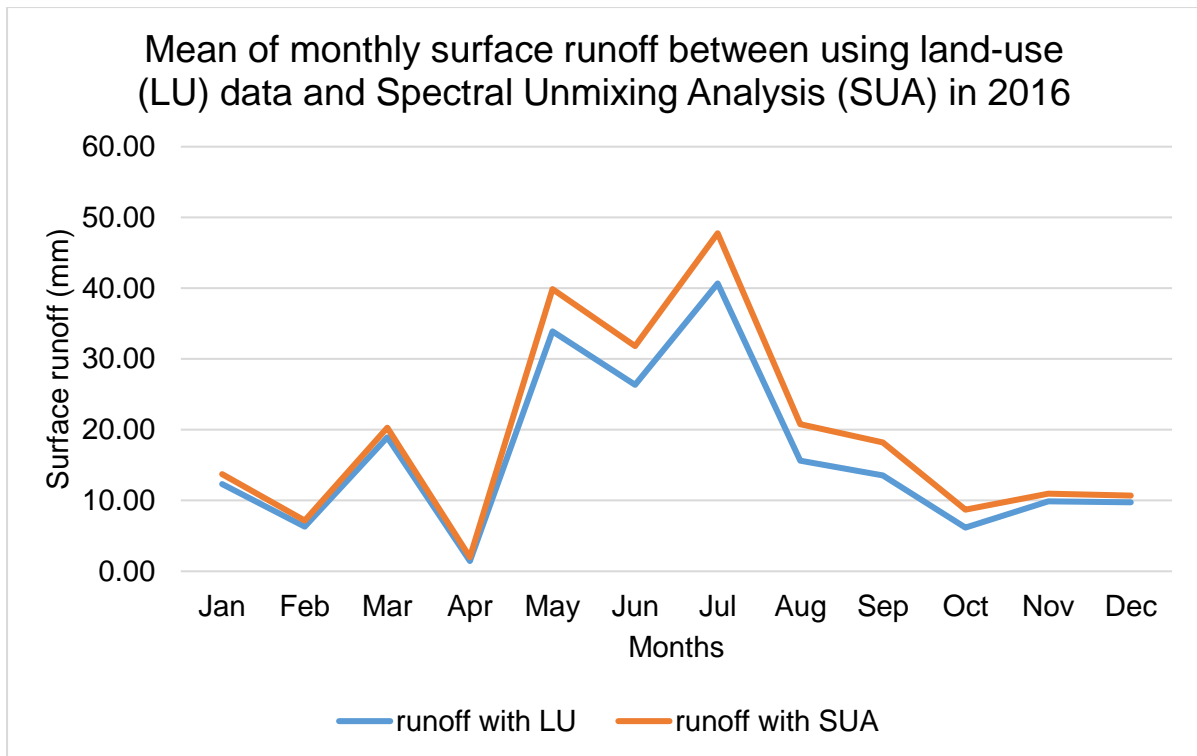


**Figure 6.7.** Mean values of monthly surface runoff resulting from using land-use map and fractional maps from Spectral Unmixing Analysis in 2016

**b. At the annual level**

The mean value of annual surface runoff derived using the land-use map and default LC fractions in WetSpass is considerably smaller than that of the derived LC fractions derived using Spectral Unmixing, which are 194.94 and 232.10 mm respectively. As discussed above in the monthly level of spatial surface runoff distribution, monthly surface runoff is likely to be underestimated using the land-use map and default LC fractions in WetSpass . Consequently, the annual surface runoff volume resulting from the sum of monthly runoff volumes is also likely to be underestimated.

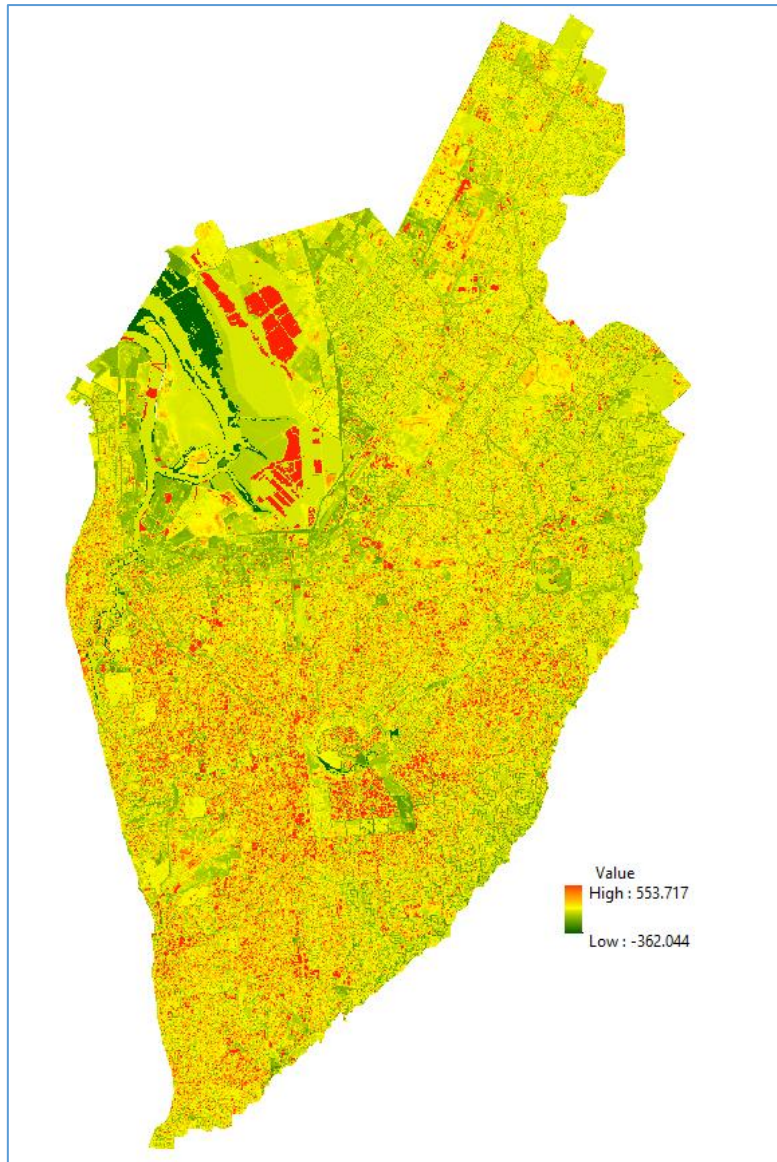


**Figure 6.8.** Differences between annual surface runoff of WetSpass using Spectral Unmixing Analysis and Land-use data

**Figure 6.8** illustrates the results of annual surface runoff of WetSpass using derived LC fractions from the Spectral Unmixing method minus the annual surface runoff of WetSpass using land-use maps and default fractions. Generally, there are some significant differences between two results.

Firstly, there are some large red areas which are salt fields in the North-East of the study area. Those areas show significantly higher values using derived fractions from the Spectral Unmixing method in WetSpass and remarkably low values using land-use and

default LC fractions in WetSpass. This issue can be explained as follows: The Landsat 8 surface reflectance image acquired on 07 January 2016 was used for conducting the supervised classification. At that time, those salt fields contained water and they were recorded on the satellite image (the red circle in **Figure 6.9**). The classification identified these areas as open water in the derived land cover map. This open water class in classification map was extracted and directly used as the fractional map of open water in WetSpass with the value of '1' for the presence of open water and '0' for the absence of water on the derived map (**Figure 5.3**). However, these same areas on the land-use map are categorised as mine-quarry (the percentage of bare soil is 100%, percentage of others is zero), industry (the percentage of vegetation and impervious surface is 40% and 60% respectively, percentage of others is zero), and agricultural land (percentage of vegetation and bare soil is 20% and 80% respectively, percentage of others is zero). Due to the difference in features that cover these areas, this leads to the significant difference in surface runoff results between methods.



**Figure 6.9.** Open water and mixed water-vegetation-bare soil areas marked on Landsat 8 Reflectance Image

Furthermore, the dark green region in **Figure 6.8** shows considerably lower values of surface runoff resulting from WetSpass using the derived LC fractions from the Spectral Unmixing method and significantly higher values when using the land-use map and default LC fractions. As recorded on the Landsat image, these areas are a mixture of water, vegetation and bare soil (the yellow circle in **Figure 6.9**). However, those areas in land-use map are river. This leads to result in high values of surface runoff results when using land-use map while the values of those areas are lower when using fractional maps.

Finally, observed differences between surface runoff results between the two approaches is scattered throughout the study area, while notably more concentrated in more heterogeneous areas where natural variation in land cover composition occurs, such as across the residential, commercial and CBD areas. This is explained by the

likely underestimation of surface runoff volumes in some urban environments when the land-use map and default LC fractions are used in the WetSpass model, as discussed above. Otherwise, the yellow colour in **Figure 6.8** demonstrates that surface runoff values between the two methods are much closer together.

With the discussion above, the results of WetSpass model using derived LC fractions from Spectral Unmixing are arguably more reasonable and more reliable than using the land-use map and default LC fractions in this research. The Spectral Unmixing results better reflect the abundance of vegetation, bare soil and impervious surfaces in heterogeneous environments like urban areas. Therefore, if land cover fractions can be accurately derived using Spectral Unmixing Analysis, these derived parameters (fractions) should replace the land-use map and default fractions in the WetSpass model.

#### **6.1.4 Areas vulnerable to surface runoff and flooding**

‘Surface runoff’ is water that flows over a land surface before accumulating in a channel, while ‘flooding’ typically occurs when the water volume exceeds the capacity of the channel and overflows into and beyond the flood plain. There are different factors affecting flooding in a catchment, such as rainfall; river characteristics, including size and nature of the river; vegetation in and around the river; downstream water levels; and stormwater drainage (The Queensland Government 2011). Identifying areas vulnerable to flooding requires research on all these causative factors relevant to each individual catchment before mitigation efforts can be applied to these areas throughout the Adelaide metropolitan area. In this study, only surface runoff is considered and vulnerability to ‘flooding’ from surface runoff largely ignores these causative factors. This might seem subjective, however, it is meaningful for urban areas where rainfall

intensity is high, the drainage system is in poor condition or is absent in areas where urban development is unplanned, as is the case in Hanoi and Ho Chi Minh City in Vietnam. The areas vulnerable to surface runoff flooding in Adelaide are shown in **Figure 6.10** and are based on high amounts of surface runoff determined by the WetSpss model using derived LC fractions from Spectral Unmixing Analysis. As **Figure 6.10** presents, the areas vulnerable to flooding have a high amount of surface runoff, such as the South-West of the City of Norwood Payneham and St Peter, the CBD area, the East of Marion adjacent to the West of Mitcham, the South-East of the City of West Torrens and the North of Charles Sturt adjacent to Port Adelaide Enfield.

Notably, there is no evidence that flooding has occurred in these areas due to surface runoff. Importantly, though these areas are identified in this study as being vulnerable to surface runoff (Figure 28) based on the LC parameters used and the assumption there is no suitable stormwater infrastructure to manage surface runoff; despite no assessment of the later in this study. Consequently, this analysis, while valid for the Adelaide urban environs, lends itself more to developing countries where urban development is uncontrolled and stormwater infrastructure is poorly planned or non-existent potentially leading to greater surface runoff vulnerability.

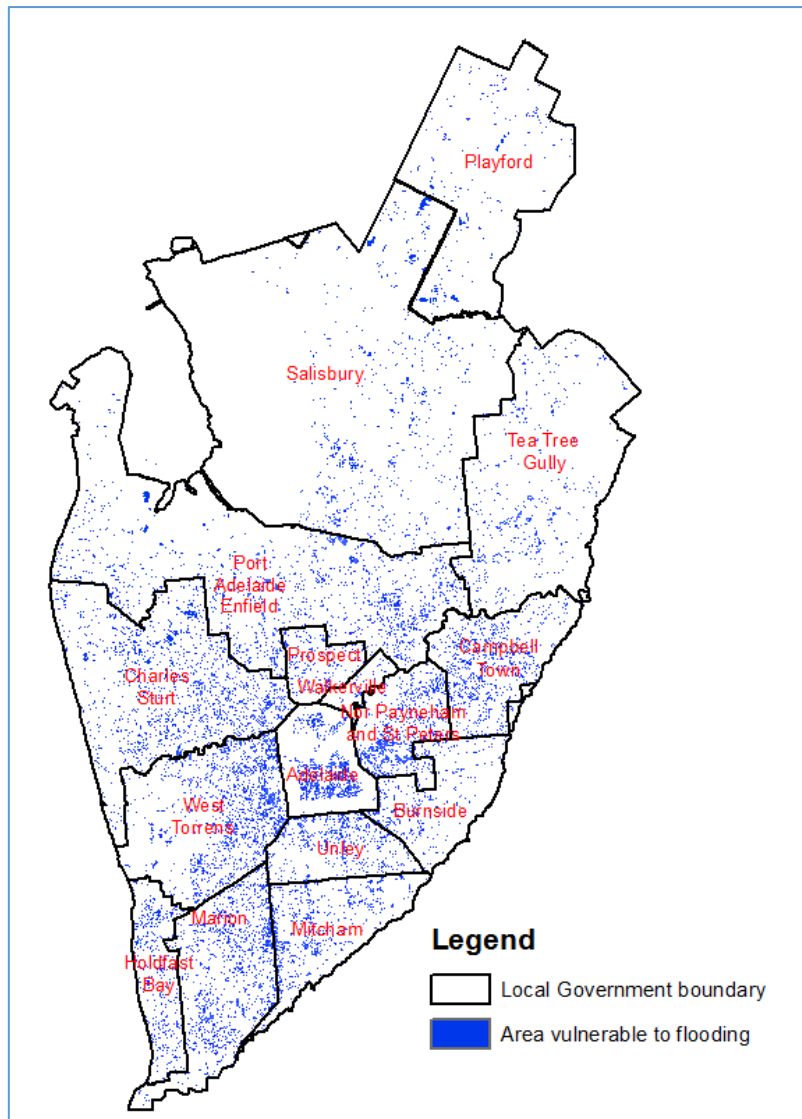


**Figure 6.10.** Areas vulnerable to flooding based on surface runoff volume

## 6.2 Limitations

The primary limitation of this study’s mythological approach is the reliance on specific spatial and environmental data necessary for the WetSpaas model, which may not be available. This study initially planned to investigate surface runoff vulnerability in Ho Chi Minh City, Vietnam, (the author’s home country) where flooding often occurs due to the high intensity of rainfall, high level of tides, and poor condition of drainage systems. Substantial progress was made to access and ‘create’ the necessary data for Ho Chi Minh City, however, its availability was limited and of much lower accuracy. Field

work would be required to improve the quality of data, which was not an option. While, discrete or fractional Land cover maps are typical products derived from remotely sensed imagery globally, land-use is a more challenging and time consuming product to acquire. Moreover, access to other spatial and environmental data necessary for the WetSpass model can be difficult, such as soil maps, elevation, groundwater depth, temperature, rainfall, wind and evapotranspiration. Access to data often requires a highly developed and rigorous data capture campaign sanctioned by the state and driven by a sophisticated spatial infrastructure industry. Accordingly, the study was changed to the Adelaide metropolitan area resulting in a more restrictive timeframe for completion, but where high quality data was available. Thus as indicated in the last section, it's unfortunate that the results from this method may best serve developing countries but where the necessary input data may not be readily available.

When conducting Spectral Unmixing Analysis, resulting composition of LC fractions that accurately sum to one (and are non-negative) require suitably accurate candidate endmember signatures as input to the linear unmixing algorithm. In this study, the purest endmember signatures were subjectively collected from training locations throughout Adelaide with the help of high resolution Google Earth imagery. While the resulting fraction images produced good results in this study, a more objective approach to signature suitability is to use ENVI's Pixel Purity Index (PPI), which arguably could improve the accuracy of the final LC fraction images prior to input to WetSpass. The PPI method uses thousands of random unit vectors (skewers) projected through the multispectral 'data cloud' where pixels found to be 'extreme' or at the edges of the data cloud are more spectrally pure and thus more representative of the endmember features

(land cover types) to be mapped. Furthermore, the results of endmember abundance (fraction images) are not validated due to the limited time of conducting the thesis. The validation for Spectral Unmixing Analysis results can be implemented by two methods, field investigation or lab-processing. In terms of a field investigation method, random validation locations in the study area are chosen to measure the proportions of vegetation, bare soil and impervious surfaces using field sampling measurements. Each location (quadrat) should have an area of 90x90 meters (8,100 m<sup>2</sup>) taking account of the geometric accuracy of the Landsat imagery of +/- one pixel for a spatial resolution of 30m. Coordinates of the four corners of the quadrat need to be recorded to adequately identify the field location in the image. The accuracy of unmixing results is determined by comparing (through correlation) the measured percentage of land cover (for each endmember) at each field location with the endmember proportions (fractions) at corresponding locations derived by the unmixing process. The lab-processing method aims to achieve the same objective comparison but high resolution imagery is used as a surrogate for field validation sites.

Finally, input data such as rainfall and temperature can be improved in accuracy by exploring the raw data before applying interpolators. A suitable interpolator can be determined by exploring the distribution of values in the raw data. In addition, research by Saveliev et al. (1998) indicates that rainfall and the natural terrain have a strong correlation. Therefore, this relationship should be considered and suitably analysed.

## **Chapter 7 - Conclusion**

This study has illustrated the application of Spectral Unmixing of Landsat imagery coupling with the hydrological model WetSpass in surface runoff estimation. In consideration of the research aim, the study modelled monthly and annually spatial distribution of potential surface runoff. In doing so the annual surface runoff resulting from the WetSpass model, derived using derived LC fractions from Spectral Unmixing Analysis, was used to identify areas vulnerable to surface runoff flooding over metropolitan Adelaide. Vulnerability in this context is determined using surface runoff volume. Importantly, to achieve the aim, the study collected and produced the input data for the WetSpass model including land-use, elevation, slope, soil types, rainfall, temperature, wind, potential evapotranspiration and groundwater depth using GIS methods. Notably, this research investigated the application of Spectral Unmixing Analysis of multispectral Landsat imagery to produce land cover fractions as input parameters to replace the default land cover proportions assigned to the land-use categories in the WetSpass model. Furthermore, the spatial distribution of surface runoff over 12 months in 2016 was mapped. The result of both methods, WetSpass using land-use and default LC data and using Spectral Unmixing Analysis, indicates higher volumes of surface runoff in the months having higher rainfall intensity. In the results shown using the land-use and default fractions, the volume of monthly surface runoff is likely to be similar in adjacent pixels where they have the same soil type, land-use and rainfall. In contrast, the results shown using the derived LC fractions vary depending on the contribution of vegetation, bare soil, impervious surfaces and open

water in those pixels. The mean values of the latter method are greater than that of the former in every month and over the whole year.

Regarding the research questions, the research findings show that fractional maps resulting from Spectral Unmixing of Landsat imagery can represent better parameters for WetSpass model in estimating surface runoff instead of using the land-use map and default LC proportions. The results from the method using land-use are likely underestimated in the Adelaide metropolitan area due to the heterogeneous landscape, while the results from the method using Spectral Unmixing Analysis are likely more reliable. Furthermore, by conducting the test of measuring the proportions of vegetation, impervious surfaces and bare soil in the fractional maps within the boundaries of Commercial and Road, and Industry land-use types, the statistics show that the results of Spectral Unmixing Analysis are reasonable and reliable. The outcomes of WetSpass using Spectral Unmixing Analysis are better than that using land-use alone in this study. In addition, this study also indicates some areas vulnerable to surface runoff flooding in the metropolitan Adelaide based on high volumes of surface runoff.

The outcomes of this study are necessary for prioritised flooding mitigation measures based on the current status of the areas vulnerable to surface runoff. This also indicates that using remote sensing and GIS method in deriving data as the input data for a hydrological model can achieve a better result. Spectral Unmixing results are also meaningful in understanding urban environment.

Lastly, there are some limitations in this research. The Pure Pixel Index should be applied with Landsat image data before conducting endmember selection to help

achieve a better result. The land cover fractional maps resulting from Spectral Unmixing Analysis also need to be validated and the raw data such as rainfall, temperature and groundwater depth need further investigation in order to identify a potentially better interpolation method for raster surface generation.

## **Recommendations**

As discussed in the Literature review section, impervious surfaces significantly affect surface runoff volume. In areas where the necessary data required for the WetSpass model is limited or of low accuracy, alternative approaches could be used to ‘indicate’ potential vulnerable areas to surface runoff. The Normalized Difference Built-up Index (NDBI) is sensitive to impervious surfaces, which are characteristic of urban environments. Thus while the NDBI is a quantitative index, where higher index values indicate the presence of more impervious surfaces, it does not provide surface runoff volumes. However, there is likely to be a correlation between the two and thus could be used as a surrogate assessment of surface runoff vulnerability where the index is easily derived using globally available data sets, for example, Landsat imagery. Furthermore, the Normalized Difference Vegetation Index (NDVI) also measures the presence of green vegetation. Therefore, future research should also consider how NDBI and NDVI can be used as the parameters for impervious surfaces and vegetation that vary over a landscape in a hydrological model.

In future research, it is also advisable to apply the WetSpass model to specific catchments separately. Research on flooding in a catchment can help to achieve more understanding of local conditions and causative factors before applying the research to

a wider area. The research also should be done in a temporal scale to investigate changes of impervious surfaces and runoff potential over time. Notably, changes in NDBI and NDVI results over time may play a role and could be used to help predict the trend of surface runoff changes. Importantly, this study demonstrates that if the appropriate data is available, WetSpass provides modelled surface runoff volumes over time and to highlight areas vulnerable to surface runoff and flooding.

## References

Abdollahi, K, Batelaan, O & Huysmans, M 2015, 'Distributed Monthly Water Balance Model: Formulation and Application on Black Volta Basin', Vrije University Brussel.

ABS 2016, *Regional Population Growth, Australia, 2014-15*, Australian Bureau of Statistics, viewed 20 Sep 2016, <<http://www.abs.gov.au/ausstats/abs@.nsf/Latestproducts/3218.0Main%20Features352014-15?opendocument&tabname=Summary&prodno=3218.0&issue=2014-15&num=&view=>>>.

Al Kuisi, M & El-Naqa, A 2013, 'GIS based Spatial Groundwater Recharge estimation in the Jafr basin, Jordan—Application of WetSpa models for arid regions', *Revista Mexicana de Ciencias Geológicas*, vol. 30, no. 1, pp. 96-109.

ArcGIS ESRI 2016, *How IDW works*, ESRI, viewed 16 October 2016, <<http://desktop.arcgis.com/en/arcmap/10.3/tools/3d-analyst-toolbox/how-idw-works.htm>>.

Arnold, JCL & Gibbons, CJ 1996, 'Impervious surface coverage: the emergence of a key environmental indicator', *Journal of the American Planning Association*, vol. 62, no. 2, pp. 243-58.

Attorney-General's Department nd, *Floods - warning, preparedness and safety*, by Attorney-General's Department.

Bahremand, A, De Smedt, F, Corluy, J, Liu, Y, Poorova, J, Velcicka, L & Kunikova, E 2007, 'WetSpa model application for assessing reforestation impacts on floods in Margecany–Hornad watershed, Slovakia', *Water Resources Management*, vol. 21, no. 8, pp. 1373-91.

Batelaan, O & De Smedt, F 2001, 'WetSpa: a flexible, GIS based, distributed recharge methodology for regional groundwater modelling', *IAHS PUBLICATION*, pp. 11-8.

Bauer, ME, Loffelholz, BC & Wilson, B 2008, *Estimating and mapping impervious surface area by regression analysis of Landsat imagery*, CRC Press, Taylor & Francis Group: Boca Raton.

Bich, TH, Quang, LN, Thanh Ha, LT, Duc, TT & Guha-Sapir, D 2011, 'Impacts of flood on health: epidemiologic evidence from Hanoi, Vietnam', *2011*, vol. 4.

Binaghi, E, Brivio, PA, Ghezzi, P & Rampini, A 1999, 'A fuzzy set-based accuracy assessment of soft classification', *Pattern recognition letters*, vol. 20, no. 9, pp. 935-48.

BOM 2016, *Annual Climate Report 2015*, Australian Government - Bureau of Meteorology, 12 Sep 2016, <[http://www.bom.gov.au/climate/annual\\_sum/2015/Annual-Climate-Report-2015-LR.pdf](http://www.bom.gov.au/climate/annual_sum/2015/Annual-Climate-Report-2015-LR.pdf)>.

Borough, P & McDonnell, R 1998, *Principles of geographical information system*, Oxford: Oxford University Press.

Boyd, M, Bufill, M & Knee, R 1993, 'Pervious and impervious runoff in urban catchments', *Hydrological Sciences Journal*, vol. 38, no. 6, pp. 463-78.

Breuer, L, Huisman, J, Willems, P, Bormann, H, Bronstert, A, Croke, B, Frede, H-G, Gräff, T, Hubrechts, L & Jakeman, A 2009, 'Assessing the impact of land use change on hydrology by ensemble modeling (LUCHEM). I: Model intercomparison with current land use', *Advances in Water Resources*, vol. 32, no. 2, pp. 129-46.

- Brooks, N 2003, 'Vulnerability, risk and adaptation: A conceptual framework', *Tyndall Centre for Climate Change Research Working Paper*, vol. 38, pp. 1-16.
- Bureau of Meteorology 2016, *Australian Water Information Dictionary*, Bureau of Meteorology, Commonwealth of Australia.
- Canters, F, Batelaan, O, de Voorde, TV, Chormański, J & Verbeiren, B 2011, 'Use of impervious surface data obtained from remote sensing in distributed hydrological modeling of urban areas', *Urban Remote Sensing: Monitoring, Synthesis and Modeling in the Urban Environment*, pp. 255-73.
- Chen, J, Hill, AA & Urbano, LD 2009, 'A GIS-based model for urban flood inundation', *Journal of Hydrology*, vol. 373, no. 1, pp. 184-92.
- Commonwealth of Australia 2009, 'Flood Preparedness', in *Australian Emergency Manual Series*, Attorney-General's Department, 3 – 5 National Circuit, BARTON ACT 2600.
- Cracknell, A 1998, 'Review article Synergy in remote sensing-what's in a pixel?', *International Journal of Remote Sensing*, vol. 19, no. 11, pp. 2025-47.
- Creutzfeldt, B, Güntner, A, Wziontek, H & Merz, B 2010, 'Reducing local hydrology from high-precision gravity measurements: a lysimeter-based approach', *Geophysical Journal International*, vol. 183, no. 1, pp. 178-87.
- Dams, J, Dujardin, J, Reggers, R, Bashir, I, Canters, F & Batelaan, O 2013, 'Mapping impervious surface change from remote sensing for hydrological modeling', *Journal of Hydrology*, vol. 485, pp. 84-95.
- Douben, KJ 2006, 'Characteristics of river floods and flooding: a global overview, 1985–2003', *Irrigation and drainage*, vol. 55, no. S1.
- Dunne, T 1986, 'Urban Hydrology in the Tropics: problems solutions, data collection and analysis', in *Urban climatology and its application with special regards to tropical areas*, *Proc. of the Mexico Tech Conf.*
- Eastman, J & Laney, R 2002, 'Bayesian Soft Classification for Sub-Pixel Analysis: A Critical Evaluation'.
- Eisensee, T & Strömberg, D 2007, 'News droughts, news floods, and US disaster relief', *The Quarterly Journal of Economics*, pp. 693-728.
- El-Kawy, OA, Rød, J, Ismail, H & Suliman, A 2011, 'Land use and land cover change detection in the western Nile delta of Egypt using remote sensing data', *Applied Geography*, vol. 31, no. 2, pp. 483-94.
- Fadil, A, Rhinane, H, Kaoukaya, A, Kharchaf, Y & Bachir, OA 2011, 'Hydrologic modeling of the Bouregreg watershed (Morocco) using GIS and SWAT model', *Journal of Geographic Information System*, vol. 3, no. 04, p. 279.
- Fisher, P 1997, 'The pixel: a snare and a delusion', *International Journal of Remote Sensing*, vol. 18, no. 3, pp. 679-85.
- Foody, G 2004, 'Sub-pixel methods in remote sensing', in *Remote sensing image analysis: Including the spatial domain*, Springer, pp. 37-49.

Footy, G & Cox, D 1994, 'Sub-pixel land cover composition estimation using a linear mixture model and fuzzy membership functions', *Remote Sensing*, vol. 15, no. 3, pp. 619-31.

Freeze, RA 1974, 'Streamflow generation', *Reviews of Geophysics*, vol. 12, no. 4, pp. 627-47.

Frizzelle, BG & Moody, A 2001, 'Mapping continuous distributions of land cover: A comparison of maximum-likelihood estimation and artificial neural networks', *Photogrammetric Engineering and Remote Sensing*, vol. 67, no. 6, pp. 693-706.

Garcia, L 2002, 'Overview of early warning systems for hydrometeorological hazards in selected countries in Southeast Asia:(Cambodia, Indonesia, Lao PDR, Philippines and Vietnam)', in Asian Disaster Preparedness Center (ADPC), Thailand.

Gerges, NZ 2006, *Overview of the hydrogeology of the Adelaide metropolitan area*, Department of Water, Land and Biodiversity Conservation.

Ghosh, G, Kumar, S & Saha, S 2012, 'Hyperspectral satellite data in mapping salt-affected soils using linear spectral unmixing analysis', *Journal of the Indian Society of Remote Sensing*, vol. 40, no. 1, pp. 129-36.

Goodchild, M 1993, *The State of GIS for environmental problem-solving. Chapter 2 in Environmental Modeling with GIS*, edited by MF Goodchild, BO Parks, and LT Steyaert, Oxford University Press.

Government of South Australia 2013, *Adelaide and Mount Lofty Ranges Natural Resources Management Plan*, by Government of South Australia, vol. 1.

Government of South Australia 2007, *Local Government (Stormwater Management) Amendment Act 2007*, viewed 12 October 2016, <[https://www.lga.sa.gov.au/webdata/resources/files/Local\\_Government\\_\(Stormwater\\_Management\)\\_Amendment\\_Bill\\_2007\\_-\\_Final\\_form.pdf](https://www.lga.sa.gov.au/webdata/resources/files/Local_Government_(Stormwater_Management)_Amendment_Bill_2007_-_Final_form.pdf)>.

Güneralp, B, Güneralp, İ & Liu, Y 2015, 'Changing global patterns of urban exposure to flood and drought hazards', *Global environmental change*, vol. 31, pp. 217-25.

Hamin, EM & Gurran, N 2009, 'Urban form and climate change: Balancing adaptation and mitigation in the US and Australia', *Habitat International*, vol. 33, no. 3, pp. 238-45.

Hanoi capital city's People Committee 2008, *Report of Hanoi capital city's People Committee on heavy rain situation, inundation, damages, and measures to overcome the situation*, Hanoi, Vietnam.

Ian, H, Sarah, C & Steve, C 2010, *An introduction to geographical information systems*, Pearson Education India.

Jensen, JR 2005, *Introductory digital image processing: A remote sensing perspective*, Pearson College Division.

Jha, AK, Bloch, R & Lamond, J 2012, *Cities and flooding: a guide to integrated urban flood risk management for the 21st century*, World Bank Publications.

Ji, M & Jensen, JR 1999, 'Effectiveness of subpixel analysis in detecting and quantifying urban imperviousness from Landsat Thematic Mapper imagery', *Geocarto International*, vol. 14, no. 4, pp. 33-41.

- Jonkman, SN 2005, 'Global perspectives on loss of human life caused by floods', *Natural Hazards*, vol. 34, no. 2, pp. 151-75.
- Kalkhan, MA 2011, *Spatial statistics: geospatial information modeling and thematic mapping*, CRC Press.
- Kellogg Brown & Root Pty Ltd 2004, *Metropolitan Adelaide Stormwater Management Study: Part A – Audit of existing information*, 186 Greenhill Road, Parkside, South Australia 5063.
- Keshava, N & Mustard, JF 2002, 'Spectral unmixing', *IEEE signal processing magazine*, vol. 19, no. 1, pp. 44-57.
- Klijin, F 2009, *Flood risk assessment and flood risk management; an introduction and guidance based on experiences and findings of FLOODsite (an EU-funded integrated project)*, Deltares.
- Koomen, E & Borsboom-van Beurden, J 2011, *Land-use modelling in planning practice*, Springer.
- Liu, Y, Zhang, HH & Wu, Y 2011, 'Hard or soft classification? Large-margin unified machines', *Journal of the American Statistical Association*, vol. 106, no. 493, pp. 166-77.
- Lu, D, Mausel, P, Brondizio, E & Moran, E 2004, 'Change detection techniques', *International Journal of Remote Sensing*, vol. 25, no. 12, pp. 2365-401.
- Lu, D, Moran, E & Hetrick, S 2011, 'Detection of impervious surface change with multitemporal Landsat images in an urban–rural frontier', *ISPRS Journal of Photogrammetry and Remote Sensing*, vol. 66, no. 3, pp. 298-306.
- Lu, D & Weng, Q 2004, 'Spectral mixture analysis of the urban landscape in Indianapolis with Landsat ETM+ imagery', *Photogrammetric Engineering & Remote Sensing*, vol. 70, no. 9, pp. 1053-62.
- Lu, D & Weng, Q 2006, 'Use of impervious surface in urban land-use classification', *Remote Sensing of Environment*, vol. 102, no. 1, pp. 146-60.
- Lu, D & Weng, Q 2007, 'A survey of image classification methods and techniques for improving classification performance', *International Journal of Remote Sensing*, vol. 28, no. 5, pp. 823-70.
- Madhavan, BB, Kubo, S, Kurisaki, N & Sivakumar, T 2001, 'Appraising the anatomy and spatial growth of the Bangkok Metropolitan area using a vegetation-impervious-soil model through remote sensing', *International Journal of Remote Sensing*, vol. 22, no. 5, pp. 789-806.
- Mather, PM & Koch, M 1999, *Front Matter*, Wiley Online Library.
- Mirza, MMQ 2011, 'Climate change, flooding in South Asia and implications', *Regional Environmental Change*, vol. 11, no. 1, pp. 95-107.
- Montzka, C, Canty, M, Kunkel, R, Menz, G, Vereecken, H & Wendland, F 2008, 'Modelling the water balance of a mesoscale catchment basin using remotely sensed land cover data', *Journal of Hydrology*, vol. 353, no. 3, pp. 322-34.
- Myint, SW, Mesev, V, Quattrochi, D & Wentz, EA 2013, 'Urban Image Classification: Per-Pixel Classifiers, Sub-Pixel Analysis, Object-Based Image Analysis, and Geospatial Methods. 10; Chapter'.

- National Geographic nd, *Floods*, National Geographic, viewed 12 October 2016, <<http://environment.nationalgeographic.com.au/environment/natural-disasters/floods-profile/>>.
- Navrud, S, Tuan, TH & Tinh, BD 2012, 'Estimating the welfare loss to households from natural disasters in developing countries: a contingent valuation study of flooding in Vietnam', *Global health action*, vol. 5.
- Pan, Y, Gong, H, Zhou, D, Li, X & Nakagoshi, N 2011, 'Impact of land use change on groundwater recharge in Guishui River Basin, China', *Chinese Geographical Science*, vol. 21, no. 6, pp. 734-43.
- Parliament of Australia 2015, 'Stormwater South Australia', PO Box 6100, Parliament House, Canberra ACT 2600.
- Phinn, S, Stanford, M, Scarth, P, Murray, A & Shyy, P 2002, 'Monitoring the composition of urban environments based on the vegetation-impervious surface-soil (VIS) model by subpixel analysis techniques', *International Journal of Remote Sensing*, vol. 23, no. 20, pp. 4131-53.
- Pidwirny, M 2006, 'Introduction to Surface Runoff', *Fundamentals of Physical Geography, 2nd Edition*, vol. 13, no. 11, p. 08.
- Poelmans, L, Van Rompaey, A & Batelaan, O 2010, 'Coupling urban expansion models and hydrological models: How important are spatial patterns?', *Land Use Policy*, vol. 27, no. 3, pp. 965-75.
- Price, R & Vojinovic, Z 2008, 'Urban flood disaster management', *Urban Water Journal*, vol. 5, no. 3, pp. 259-76.
- Richards, JA 1999, *Remote sensing digital image analysis*, vol. 3, Springer.
- Ridd, MK 1995, 'Exploring a V-I-S (vegetation-impervious surface-soil) model for urban ecosystem analysis through remote sensing: comparative anatomy for cities†', *International Journal of Remote Sensing*, vol. 16, no. 12, pp. 2165-85.
- Rumynin, VG 2015, 'Surface Runoff Generation, Vertical Infiltration and Subsurface Lateral Flow', in *Overland Flow Dynamics and Solute Transport*, Springer, pp. 3-50.
- Russell, K & Drew, J 2006, *Port Adelaide seawater & Stormwater flood risk treatment*, City of Port Adelaide Enfield.
- Saveliev, AA, Mucharamova, SS & Piliugin, GA 1998, 'Modeling of the daily rainfall values using surface under tension and kriging', *Journal of Geographic Information and Decision Analysis*, vol. 2, no. 2, pp. 52-64.
- Shimabukuro, Y, Carvalho, V & Rudorff, B 1997, 'NOAA-AVHRR data processing for the mapping of vegetation cover', *International Journal of Remote Sensing*, vol. 18, no. 3, pp. 671-7.
- Shimabukuro, YE & Smith, JA 1991, 'The least-squares mixing models to generate fraction images derived from remote sensing multispectral data', *IEEE TRANSACTIONS ON GEOSCIENCE AND REMOTE SENSING*, vol. 29, no. 1, pp. 16-20.
- Singh, V & Fiorentino, M 2013, *Geographical information systems in hydrology*, vol. 26, Springer Science & Business Media.

Slonecker, ET, Jennings, DB & Garofalo, D 2001, 'Remote sensing of impervious surfaces: A review', *Remote Sensing Reviews*, vol. 20, no. 3, pp. 227-55.

Small, C 2004, 'The Landsat ETM+ spectral mixing space', *Remote Sensing of Environment*, vol. 93, no. 1, pp. 1-17.

Storch, H & Downes, NK 2011, 'A scenario-based approach to assess Ho Chi Minh City's urban development strategies against the impact of climate change', *Cities*, vol. 28, no. 6, pp. 517-26.

Szöllösi-Nagy, A & Zevenbergen, C 2005, *Urban Flood Management*, A.A. Balkema.

The Queensland Government 2011, *Understanding floods: Questions and Answers*, Office of The Queensland Chief Scientist.

Turc, L 1955, 'Le bilan d'eau des sols. Relations entre le précipitations, l'évapotranspiration potentielle', in *Annales Agronomiques*, vol. 1.

U.S. Department of Commerce 2005, *Floods - The awesome power*, by U.S. Department of Commerce.

UN 2006, *World urbanization prospects: the 2005 revision*, United Nations Publications.

UN 2009, *World urbanization prospects: the 2007 revision*, Document ESA/P/WP/205, Population Division of the Department of Economic and Social Affairs, New York.

UN 2015, *World Urbanization Prospects: The 2014 Revision*, New York: United Nations Department of Economics and Social Affairs, Population Division.

Vietnam Government Portal 2016, *Geographical information of Vietnam*, viewed 11 October 2016, <<http://www.chinhphu.vn/portal/page/portal/chinhphu/NuocCHXHCNVietNam/ThongTinTongHop/dialy>>.

Weng, Q 2001, 'Modeling urban growth effects on surface runoff with the integration of remote sensing and GIS', *Environmental management*, vol. 28, no. 6, pp. 737-48.

WHO 1988, 'Urbanization and its implications for child health: potential for action'.

Wilkinson, J, Hutson, J, Bestland, E & Fallowfield, H 2004, 'Audit of contemporary and historical quality and quantity data of stormwater discharging into the marine environment, and field work programme'.

World Health Organization 2013, 'Floods in the WHO European Region: health effects and their prevention'.

Wright, C & Kemp, D 2016, 'The Reality of flood forecasting in Greater Metropolitan Adelaide—maximising forecast response time', paper presented to 2016 Floodplain Management Australia Conference.

Wulder, MA, White, JC, Goward, SN, Masek, JG, Irons, JR, Herold, M, Cohen, WB, Loveland, TR & Woodcock, CE 2008, 'Landsat continuity: Issues and opportunities for land cover monitoring', *Remote Sensing of Environment*, vol. 112, no. 3, pp. 955-69.

Xian, GZ 2015, *Remote Sensing Applications for the Urban Environment*, vol. 12, CRC Press.

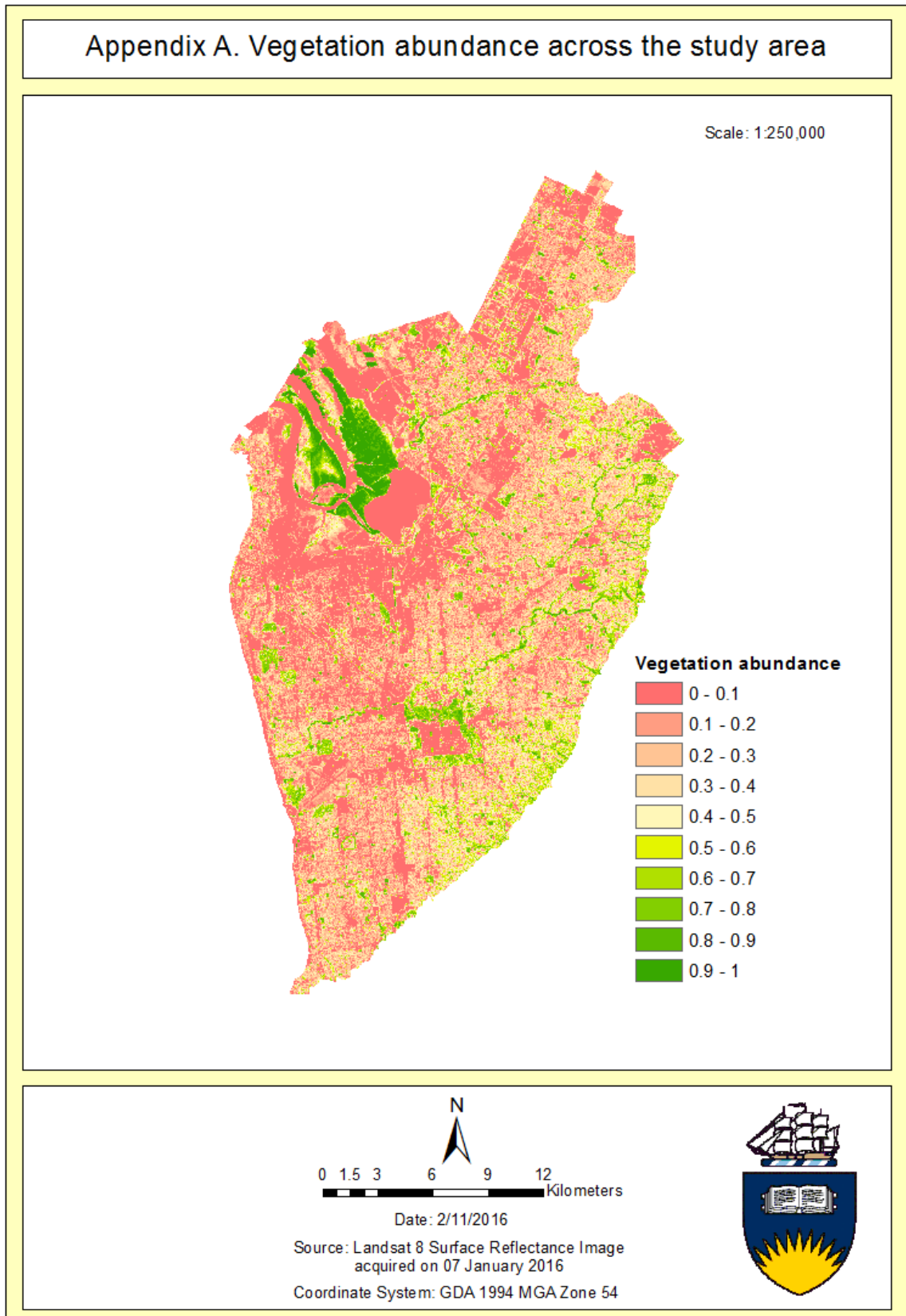
Xingnan, Z & Göran, L 1997, 'Development of an automatic calibration scheme for the HBV hydrological model', *Hydrological Processes*, vol. 11, no. 12, pp. 1671-82.

Yang, C, Everitt, JH & Du, Q 2010, 'Applying linear spectral unmixing to airborne hyperspectral imagery for mapping yield variability in grain sorghum and cotton fields', *Journal of Applied Remote Sensing*, vol. 4, no. 1, pp. 041887--11.

Yang, X & Lo, C 2002, 'Using a time series of satellite imagery to detect land use and land cover changes in the Atlanta, Georgia metropolitan area', *International Journal of Remote Sensing*, vol. 23, no. 9, pp. 1775-98.

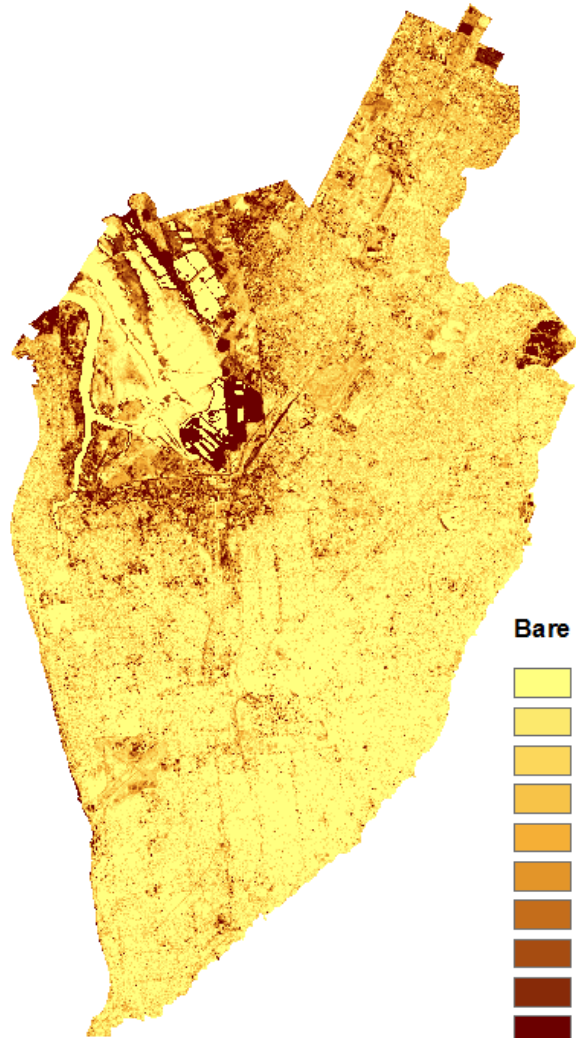
Zhang, L, Walker, GR & Dawes, WR 2002, 'Water balance modelling: concepts and applications', *Aciar Monograph Series*, vol. 84, pp. 31-47.

# Appendices

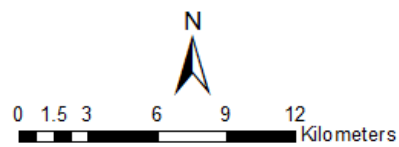
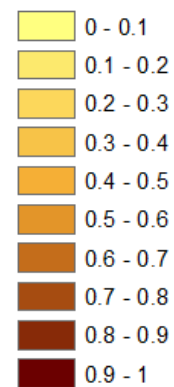


## Appendix B. Bare soil abundance across the study area

Scale: 1:250,000



### Bare soil abundance



Date: 2/11/2016

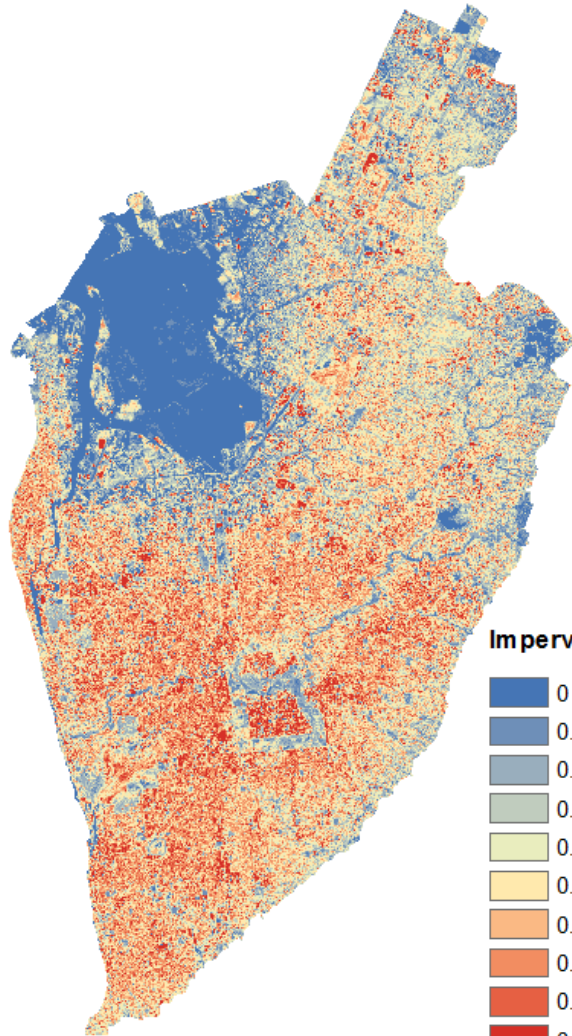
Source: Landsat 8 Surface Reflectance Image  
acquired on 07 January 2016

Coordinate System: GDA 1994 MGA Zone 54

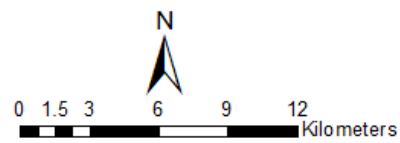
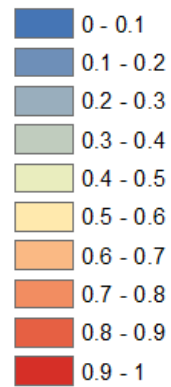


## Appendix C. Impervious surfaces abundance across the study area

Scale: 1:250,000



### Impervious surface abundance



Date: 2/11/2016

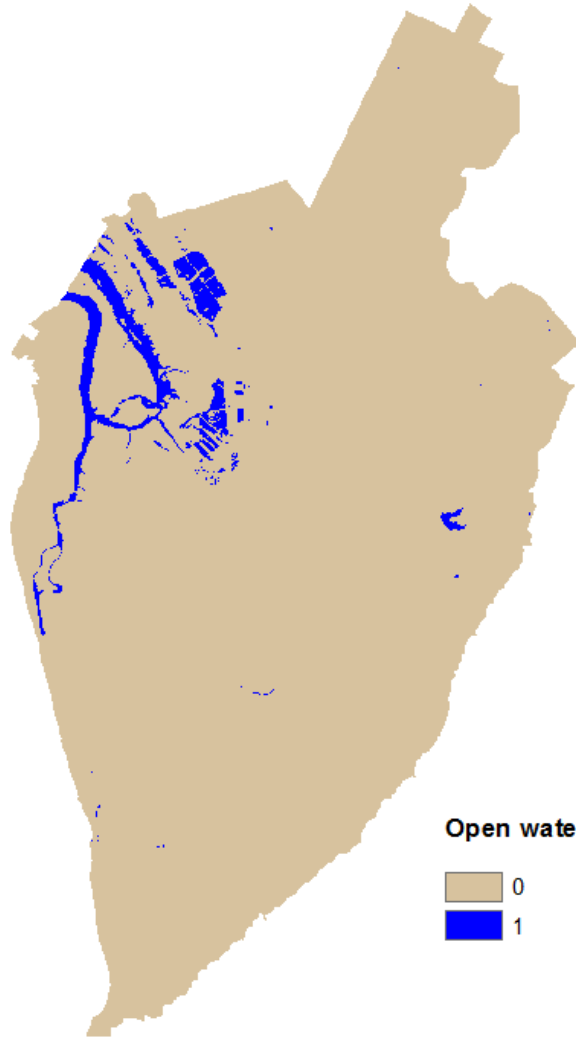
Source: Landsat 8 Surface Reflectance Image  
acquired on 07 January 2016

Coordinate System: GDA 1994 MGA Zone 54

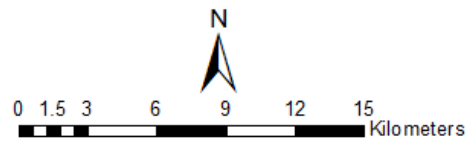


## Appendix D. Water distribution across the study area

Scale: 1:250,000



**Open water abundance**



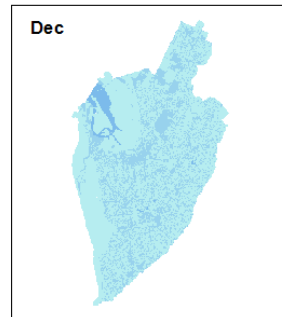
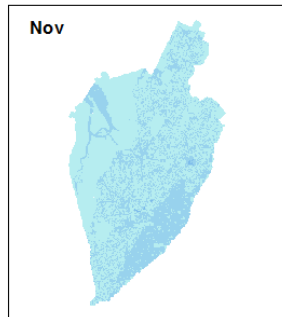
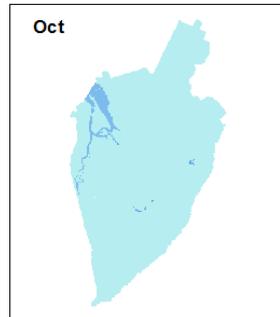
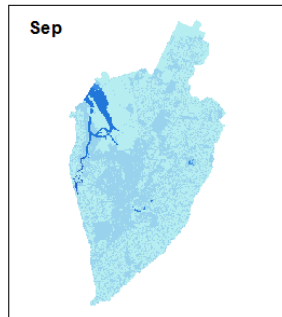
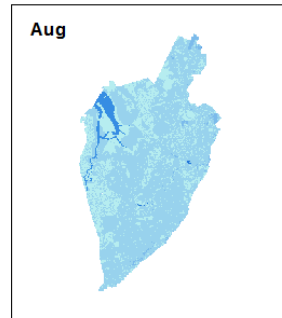
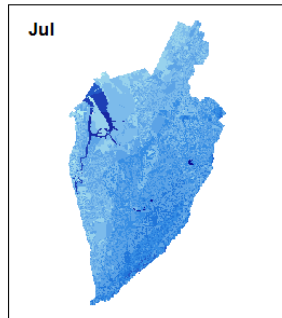
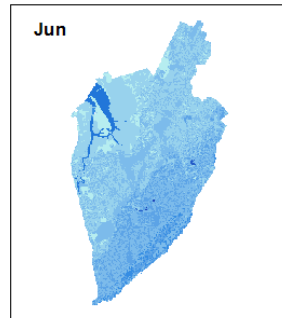
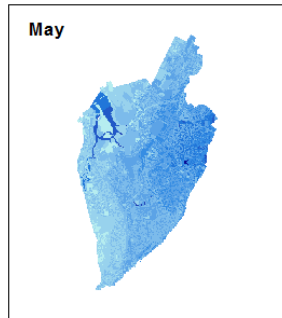
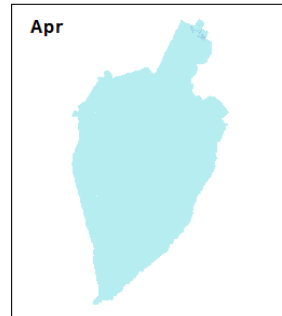
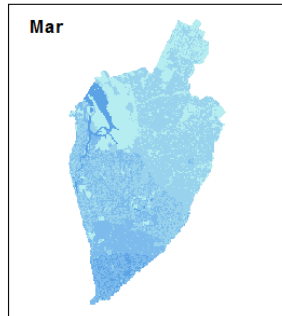
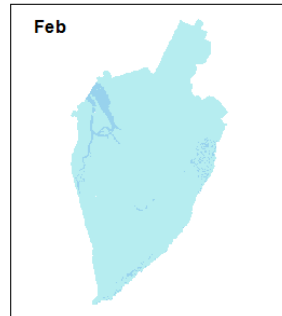
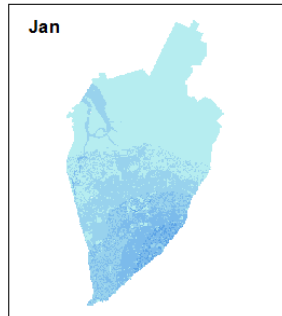
Date: 2/11/2016

Source: Landsat 8 Surface Reflectance Image  
acquired on 07 January 2016

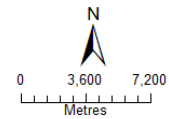
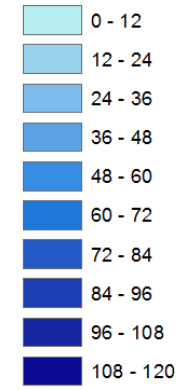
Coordinate System: GDA 1994 MGA Zone 54



Appendix E. Monthly spatial distribution of surface runoff in Adelaide 2016 using default setting of WetSpass

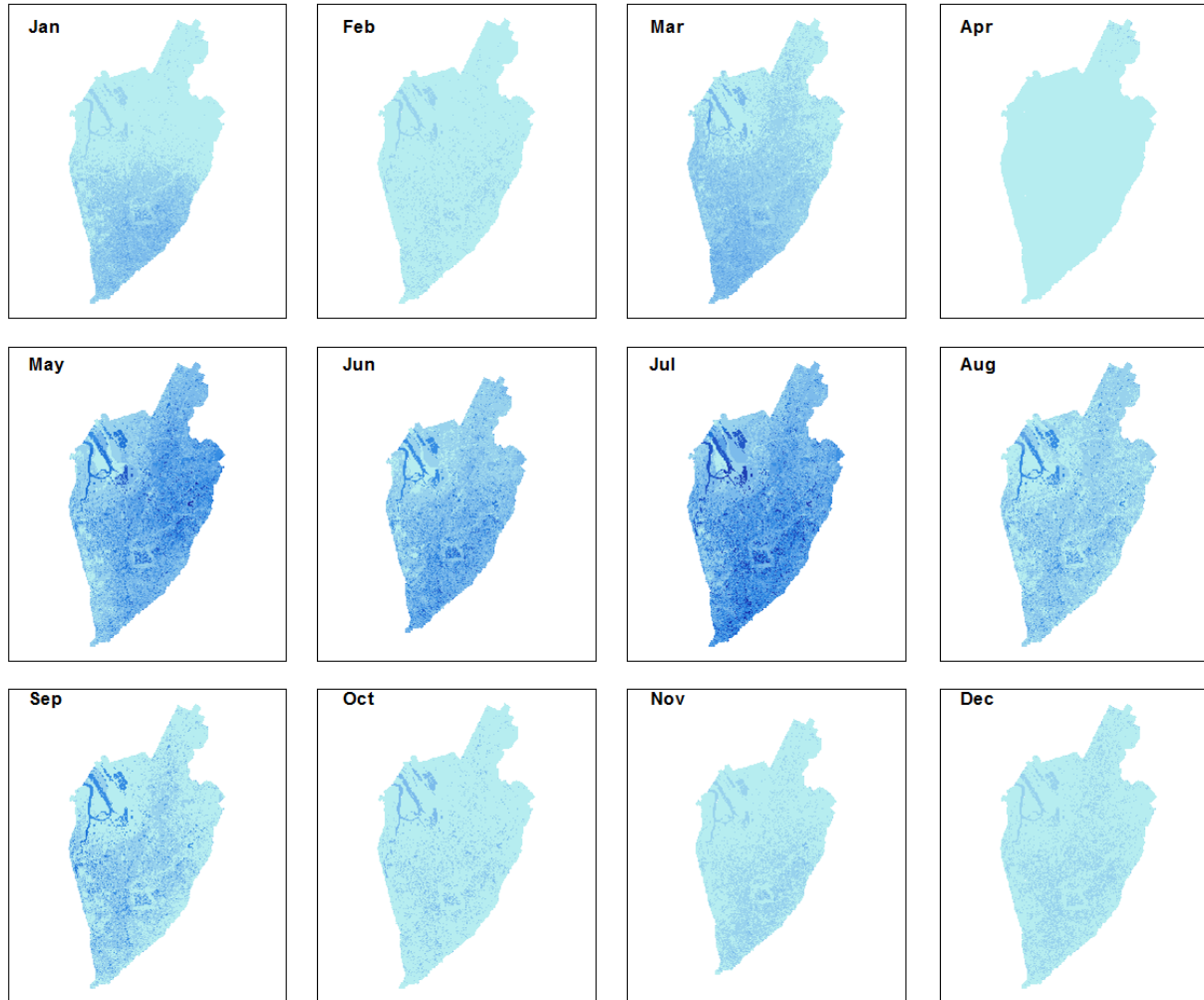


Surface runoff (mm)

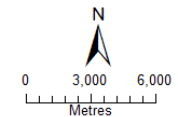
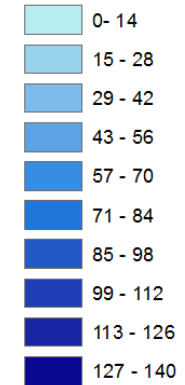


Date: 2/11/2016  
Source: Landsat 8 Surface Reflectance Image acquired on 07 January 2016  
Coordinate System: GDA 1994 MGA Zone 54

Appendix F. Monthly spatial distribution of surface runoff in Adelaide 2016 using Spectral Unmixing Analysis



Surface runoff (mm)



Date: 2/11/2016

Source: Landsat 8 Surface Reflectance Image acquired on 07 January 2016

Coordinate System: GDA 1994 MGA Zone 54